Investigation of Supersonic Panel Flutter with the Finite Element Method using Plate Elements

FOR CODE AND ADDITIONAL CONTENT, VISIT THE PROJECT GITHUB

https://github.com/TalalBukhammas/FYP

Talal AE. Bukhammas*
Department of Aeronautical and Automotive Engineering,
Loughborough University, Leicestershire LE11 3TU, UK

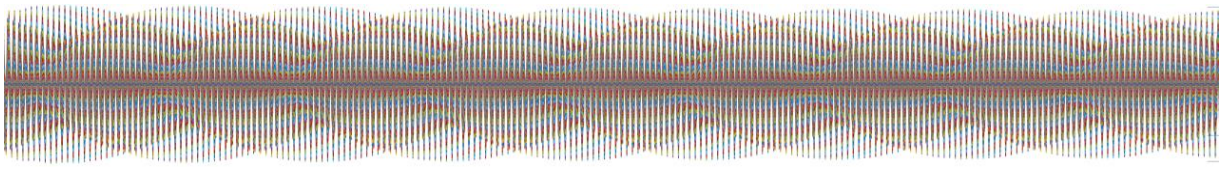

Supersonic panel flutter is a self-excited oscillatory phenomenon caused by a coupling of aerodynamic, elastic and inertial forces in supersonic flow. It occurs at some critical pressure parameter λ_{cr}, which can be associated to a critical Mach number M_{cr}. At this point, the amplitude is constant through time. Past this point, the amplitude begins to increase with time. These motions create additional stresses which can decrease panel life due to fatigue or even through rapid catastrophic failure. Additionally, any displacements made can negatively impact aerodynamic and control surface behaviour. Thus, it is critical for designers to be able to predict and mitigate this behaviour. Experimental methods and CFD simulations have proven to be costly, so more economical methods are desired. There exist commercial tools such as NASTRAN which accomplish this, however, the diversity of these tools becomes a hinderance to researchers prototyping new methods. Hence, there is a need for a free software which would allow for researchers to focus on experimentation.

This paper presents a thorough mathematical procedure in developing a Finite Element Method solver for the flutter critical pressure parameter of panels. It is written to be understandable by a Part C Aeronautical Engineering student. Two structural theories were implemented: Reissner-Mindlin plate theory for isotropic plates and first order shear deformation theory for composite laminates. Both were modelled with quadratic quadrilateral plate elements. Regarding aerodynamics, first order piston theory was used. These are combined and solved using a frequency-domain approach, which allows for significantly quicker solution times compared to CFD. Further improving on efficiency, a modal reduction technique is employed to control the dimensionality of the eigenvalue problem –for users to balance accuracy against computational time. Moreover, techniques such as reduced integration and sparse matrices were utilised to provide additional computational efficiency whilst maintaining good solution accuracy.

Good agreements were made with literature, justifying the many simplifications made throughout the project. This includes the comparison between first order piston theory and third order piston theory, where the first order piston theory implementation was validated. Although a proper time study was not performed, all solutions were obtained in less than 5 seconds which is much quicker than solutions expected from coupling CFD with structural theory. Further work involves including thermal effects, buckling, pre-stressed panels, other aerodynamic models and shells. Shells would be a major inclusion as it would allow the modelling of non-flat surfaces. However, it is believed that the detailed derivations in the paper should allow the reader to implement this in future if desired. Finally, the code should be restructured to better enable modifications. Once complete, thorough code documentation should be created to guide users and researchers.

* Aeronautical Engineering MEng; B930160; Project supervisor: Prof S. Wang

1. Introduction

Supersonic panel flutter is a self-excited oscillatory phenomenon caused by a coupling of aerodynamic, elastic and inertial forces in supersonic flow [1], [2]. This occurs at some critical dynamic pressure λ_{cr}, which is associated to a certain free-stream Mach number for linear structural theory [1]. Below the critical dynamic pressure, panel motion due to turbulence is of order less than the panel thickness [2]. Conversely, past this point, the amplitude of motion increases exponentially with time to be of order or larger than the panel thickness, however is limited due to structural non-linearities [1], [2]. Hypersonic panel flutter is similar to supersonic panel flutter but occurs at hypersonic flows instead. The study of supersonic panel flutter is highly tied to the study of hypersonic panel flutter due to the similarity of the mathematics and given that hypersonic vehicles must also operate in the supersonic regime.

Supersonic/hypersonic flutter has been of large interest since the development of hypersonic vehicles and re-entry vehicles as it can be a seed for failure [1], [3]. There exist at least three failure modes of flutter: change in vehicle dynamics triggering unpredictable behaviour, sudden structural failure as the material exceeds its failure stress state [2], [4] or cyclic loading causing long-term failure [2], [4]. Some famous examples include the X-15 and X-20 which required additional stiffening as the flutter was deemed destructive [2]. Contrarily, the Titans and S-IVB also experienced flutter, but to a lower degree so no mitigation was imposed [2]. However, these were single-use vehicles; with humanity's current endeavours towards full spacecraft reusability, such as with the recent Falcon 9 [5], an extra emphasis is now placed on further mitigating flutter to prevent fatigue failure. To accomplish this, the main objective of the designer is to increase the critical flutter Mach number above that of the principal flight envelope. Following this, the designer must then have access to rigorous prediction and mitigation tools to be certain of the safety of the vehicle before deployment whilst minimising mass penalties [2]. Moreover, to promote an iterative design workflow, these tools should be economically and temporally efficient.

Vehicle skin panels are characteristically thin sheets, with two dimensions dominating the other. These can be modelled by shell elements [1], [6], [7], which are an extended variant of plate elements. Due to time constraints, this project will concentrate on plate elements for simplicity.

Experimental aeroelastic and aerothermalelastic analysis through scaled wind tunnel testing is very involved [2], [8]. Hence, there is a desire for rapid and economical numerical models [2], [8] which can model different variations of complex geometries of spacecraft. [2], [4] focused on numerical methods. However, their methods did not extend well for complex geometries. However, [1], [9]–[14] successfully utilised FEM, which is a well-established method for solving differential equations over complex domains. As such, FEM will be the focus of this project. There is currently no publicly accessible framework in which researchers can easily implement and evaluate different theories for supersonic/hypersonic flutter. Several commercial software such as NASTRAN do provide aeroelastic analysis tools. In fact, NASTRAN even provides a comprehensive documentation on their aeroelastic tools [11]. However, researchers are limited to these tools and although modifications can be made, this process is more involved.

The main aim of the project is to program and test a Finite Element Method based solver to predict the critical flutter dynamic pressure λ_{cr}, the vibration mode shapes and natural frequencies of isotropic and composite laminate panels under supersonic flow. This was programmed in MATLAB using generality techniques such that it can be applied to more complex meshes and to also facilitate improvements in the future. This framework was then

rigorously evaluated with empirical data. This tool is not designed to replace commercial software as this is unrealistic. It is merely designed to be a tool to assist researchers. Finally, if time allows tests should be run to suggest design criteria towards minimising flutter. Due to time constraints, thermal effects, large deflections, buckling, angle of attack and aerodynamic viscous effects will be neglected. These are indeed critical in the supersonic/hypersonic flutter problem. Thus, it is encouraged to develop this project in the future to include the effects of these in the analysis. Literature for these exist do exist. [1], [8], [12], [13] consider thermal effects, [9], [12], [13] consider von-Kármán nonlinear strains and [8] considers aerodynamic viscous effects.

This technical report aims to give a detailed mathematical approach in deriving the FEM solver for supersonic flutter analysis of plates. Whilst doing research, there was not much digestible information on full FEM implementations of plates, yet alone for flutter of these plates. Moreover, many of the mathematical techniques were assumed to be known, with little information on the derivations of these. However, it should be argued that knowledge in these is valuable, as it provides understanding of when these techniques are applicable and more importantly, inapplicable. Hence, although flutter was the focus of this project, much of this report will be dedicated towards guiding the reader through the detailed derivations. This is to comply with the requirement that the report should assume knowledge of a Part C Aeronautical Engineering student.

Regarding the structure of this report, firstly, the project background will be detailed. This will give the reader context on this project. Next, the setup of integration using Gaussian Quadrature will be mathematically detailed. This will include the derivation of the shape functions of the quadratic quadrilateral element. Then, the FEM formulations of Reissner-Mindlin theory and first order shear deformation theory will be given. Next, the boundary conditions and the sparse matrix approach will be detailed. This sparse matrix approach will be one factor in improving efficiency. Next, the equations will be setup for vibrational analysis in the frequency domain. Then, the aerodynamic stiffness matrix will be derived using first order piston theory to include aerodynamic effects. Using this over CFD allows solving this easily in the frequency domain, and thus a significantly quicker solution. Next, the modal reduction technique used by [4], [12], [13] will be derived. Then, the flutter solution results will be detailed. This will return the critical flutter parameter λ_{cr}, the flutter frequency ω_{cr} and the modeshapes. The first parameter can be used to detect the occurrence of flutter, whilst the other two can be used to suggest where to alter the design to mitigate it. Finally, the conclusion & further work section will summarise the outcomes of this project and suggest further work to improve upon this project.

2. Background

2.1. Project Background

Firstly, to provide a bit of background on this project - it was initially decided to study hypersonic panel flutter. Thus, nonlinear third order piston theory aerodynamics analysis of isotropic panels was chosen. However, upon further research, it was determined that the experimental data available on hypersonic flutter was limited. Thus, it would be difficult to perform rigorous tests on the code. This was expected, but underappreciated as experimental testing of hypersonic flutter is significantly more costly than supersonic flutter. So, first order piston theory was chosen instead to simplify the solution. The extra time was spent deriving and coding first order shear deformation, after coding the linear Mindlin flutter solver.

2.2. Structural Modelling

Plate theories model the behaviour of the entire plate through its mid-surface. This simplification is analogous to modelling beams as a neutral axis, providing great computational efficiency whilst maintaining accuracy. Hence why plates are chosen over brick elements. Typical plate models employed by prior literature will be listed in increasing difficulty and discussed.

Classical Plate Theory (CPT/Kirchoff Plate Theory)

This theory was employed by [1] with results that match with literature and ANSYS analysis. CPT neglects shear and normal deformations [6], [7], [15]. [16] states that these assumptions cause CPT to overestimate buckling loads and natural frequencies and underestimate deflections for thick plates. Consequently, CPT is only suitable for thin plates. No consistent recommended thickness to span ratio range from thick vs thin was found in literature. Hence, if CPT is to be used, an investigation into this must be made.

Reissner-Mindlin Plate Theory

This theory is only valid for isotropic thick/thin plates.

No papers were found to use this as they instead opted for first order shear deformation theory. This is because FSDT works for laminates, which are better suited for supersonic/hypersonic vehicles. The theory is similar to FSDT, but treats bending and shear deformations as separate, which is unapplicable to laminates.

First Order Shear Deformation Theory (FSDT)

This will deal with orthotropic materials, where the material properties in each direction may be different. More specifically, the laminates will feature layers stacked at different angles. Thus, bending and shear contributions are now coupled.

This theory was employed by [4], [9] with close comparison to experimental data. FSDT assumes linear through-thickness in-plane displacements [7], [15], [16]. This leads to constant shear stresses and strains throughout the thickness [16]. Thus, a shear correction factor is required. [4] successfully used a value of 5/6.

Higher Order Shear Deformation Theory (HSDT)

[13] utilised HSDT with good match to empirical data. HSDT assumes higher order variations of through-thickness displacement [15], [17]. [17] compared this theory with CPT using the finite element method. For thin isotropic plates, the theories are similar but for thick anisotropic plates the discrepancies begin to emerge [17]. Furthermore, for vibrational analysis, CPT drastically underestimates the bending-stretching coupling [17]. Since this project aims to perform vibrational analysis, it is expected that HSDT would provide more accurate results than CPT and FSDT.

Discussion

Reissner-Mindlin and FSDT will be utilised (separately) as they are easier to implement over the classical theories whilst being more applicable for thicker plates. Mindlin theory is simpler and less computationally expensive than FSDT at the cost of being inapplicable to laminates. Therefore, it will be valuable in building a solid code foundation. It will also be insightful to test as no literature was found to use this in the flutter solution. With this, since HSDT is used, it is expected that the flutter solution will diverge as the thickness to span ratio increases.

2.3. Aerodynamic Modelling

Due to limited computational resources in the past, researchers have avoided the use of CFD in favour of alternative, less computationally expensive models [8]. Specific tayloring to match flight conditions leads to close comparison between these models, CFD and experimental data [8], [12]. Although Moore’s law has led to current computational power (2023) to be much larger than when flutter research started in the 1950’s, these methods still

have merit due to their accuracy and efficiency. Thus, for brevity CFD will be neglected. Attention is diverted to [8] for details on CFD methods. Furthermore, [10], [11], detail alternative advanced aerodynamic models, some proven through analysis for the NASA Space Shuttle programme.

Common inviscid supersonic/hypersonic aerodynamic models are catalogued below. Although an appreciation of the mechanics behind them are certainly beneficial, this will not be emphasised due to time-constraints.

Piston Theory

Piston theory is the most common choice in open literature for supersonic/hypersonic flutter [2], [8]. Three popular variations are [18]:

1. Lighthill's (Linear) Piston Theory
2. Van Dyke's (Second-Order) Piston Theory
3. Donov's (Third-Order) Piston Theory

All these methods involve a quasi-steady flow. [9] employed linear piston-theory and [10], [12], [13] employed third-order piston theory. Finally, [4] employed second-order piston theory. All these obtained results which matched empirical data. However, the use case is important. Linear piston theory diverges from reality with increasing Mach numbers [8]. Second-Order piston theory offers improved accuracy over linear piston theory for lower Mach numbers yet converges towards it for higher Mach numbers [8], [18].

Unsteady Newtonian-Impact Theory

This has been discussed by [8], however it is not commonly implemented. With this, [8] claims that t is accurate for large Mach numbers. Thus, it would be insightful to investigate this method..

Discussion

Some consideration on Unsteady Newton-Impact theory was made since it has not been largely used and provides great accuracy for hypersonic flow. Ultimately, doing this would force the scope of the project to be too large. Additionally, since validation for hypersonic flow is limited, the evaluation is limited to supersonic flows. Thus, it is expected for third order piston theory to give the same result as first order. Therefore, first order piston theory was chosen since it is simpler to implement.

2.4. Numerical Methods

The first solutions to the flutter problem were analytical [10]. However, these prove difficult to model complex geometries with. So, researchers began to discretise the space and solve using the Rayleigh-Ritz and the Galerkin methods [10]. Then, researchers began formulating the solution in the FEM reference frame, which improved the modelling of complex geometries [2]. More specifically, FEM was previously employed by [1], [12]–[14] with good match to empirical data.

[1], [12], [13] used the frequency domain approach whilst [9] used the time domain approach. The frequency domain approach allows for incredibly rapid solution times as the modes and modeshapes can be extracted directly. However, it is simpler to extract absolute amplitudes at certain times with the time domain approach. This is why [9] chose this approach.

[12], [13] utilised the modal reduction technique, which allowed for controlling the dimensionality of the eigenvalue problem – thereby allowing users to balance accuracy and solution time. For very fine domains, this method will bound the eigenvalue problem, preventing memory issues as well.

Discussion

For speed, the frequency domain approach and modal reduction technique will be used. For diversity in applicable problems, FEM will be used.

2.5. Linearity

[13] employed non-linear structural analysis (Von Kármán large deflection plate theory). Table 1 also demonstrates that in the hypersonic region (M>5), non-linear structural theory should be employed. However, [2] claims that this is primarily necessary for curvature into flow, buckling and pressurisation and panels already in the flutter regime [2]. Since the main aim of this project is to determine the critical dynamic pressure, where displacements are still small, and the other listed effects from [2] are neglected, it is hypothesised that the displacements will be small. Thus, linear elasticity can be assumed. This is further backed-up with the success of first order piston theory in the supersonic/hypersonic flutter analysis of [4].

Table 1: Summary of linearity of theories and their applications. Modified from [12]

Structural Theory	Aerodynamic Theory	Range of Mach No.
Linear	Linear Piston	$\sqrt{2} < M_\infty < 5$
Linear	Linearised Potential Flow	$1 < M_\infty < 5$
Non-linear	Linear Piston	$\sqrt{2} < M_\infty < 5$
Non-linear	Linearised Potential Flow	$1 < M_\infty < 5$
Non-linear	Non-linear Piston	$M_\infty > 5$
Non-linear	Euler or Navier Stokes Equations	Transonic, Supersonic and Hypersonic

With this, if a linear solution is employed, the eigenvalue problem can be solved simply. However, if non-linear methods are utilised, iterative techniques must be employed. The most common being the Newton-Raphson iterative method [19]. NASTRAN also have a range of methods to solve these non-linear aeroelastic problems [11]. Since linear methods will be used, this will not be required.

2.6. Project Contribution

Admittedly, this project is not mathematically ground-breaking. Each individual part has existed for decades. However, it does uniquely combine quadratic quadrilateral elements, Reissner-Mindlin, FSDT, first order piston theory, sparse matrix approach and the modal reduction technique in the frequency domain whilst working from first principles. Moreover, the main innovation with this project is in the code, which is not detailed in this paper. With this, it is hopeful that this project is useful to researchers.

3. Technical Achievement

3.1. 8-Noded Quadrilateral Isoparametric Elements

Integral Co-ordinate Transformation

The integration of general quadrilateral elements, as illustrated in Figure 1, is non-trivial due to the dependence of one integration limit on the other. To address this issue, a transformation of the element into the natural coordinate system is employed, wherein the integration limits are set as -1 to 1 along both axes. Figure 2 depicts this transformed element, known as the isoparametric element. This technique parallels the advantage of integrating to calculate the area of a circle more easily in polar coordinates as compared to Cartesian coordinates.

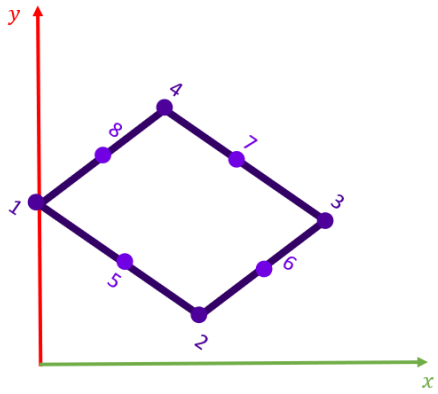

Figure 1: Element in global co-ordinate system.

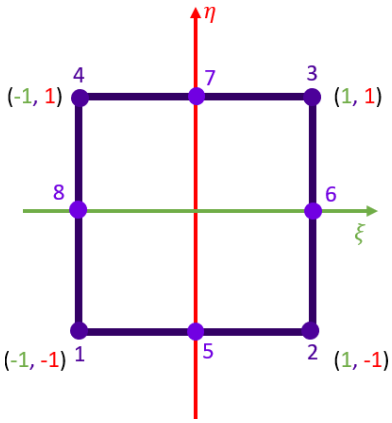

Figure 2: Element in natural co-ordinate system.

For the derivation, it is critical to maintain the node numbering scheme in Figure 2. Let ϕ represent any property measured in the element. Suppose it is desired to take the integral of this property over the element. The conversion should then exist:

$$\oiint \phi(x,y)dxdy = \int_{-1}^{1}\int_{-1}^{1} C\phi(\xi,\eta)d\xi\, d\eta \tag{1}$$

Where C is a scaling factor to incorporate the change in area of the element from Figure 1 to Figure 2.

Expressing ϕ in terms of ξ and η is straightforward since they can be represented as a linear combination of the shape functions N associated with the isoparametric element (which will be derived later in this section) and the nodal coordinates of the element in Figure 1:

$$\begin{bmatrix} x \\ y \end{bmatrix} = \begin{bmatrix} N_1 & 0 & N_2 & 0 & \dots & N_8 & 0 \\ 0 & N_1 & 0 & N_2 & \dots & 0 & N_8 \end{bmatrix} \begin{bmatrix} x_1 \\ y_1 \\ x_2 \\ y_2 \\ \dots \\ x_8 \\ y_8 \end{bmatrix} \tag{2}$$

Where N are functions of ξ and η. x_i and y_i are the nodal co-ordinates of the element in Figure 1.

These can be substituted into the function $\phi(x,y)$, which puts the integral in the form of

$$\int_{-1}^{1}\int_{-1}^{1} C\phi(\xi,\eta)dx\, dy$$

Next, the substitution for dx and dy need to be found. To do this, consider a small area in natural space. Then, consider transforming that area into global space. This can be seen going from Figure 3 to Figure 4.

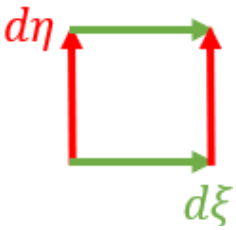

Figure 3: Area of element in natural space.

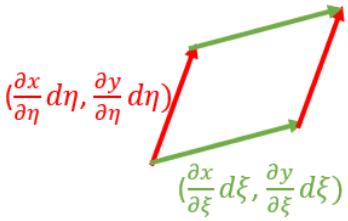

Figure 4: Area of element in global space.

The area of the element in Figure 3 is a square. Therefore, its area is given as:

$$dA_1 = d\xi \times d\eta$$

The corresponding area in Figure 4 forms a parallelogram. Therefore, it's area can be calculated as the cross product of the two vectors:

$$dA_2 = \begin{Bmatrix} \frac{\partial x}{\partial \xi} d\xi \\ \frac{\partial y}{\partial \xi} d\xi \end{Bmatrix} \times \begin{Bmatrix} \frac{\partial x}{\partial \eta} d\eta \\ \frac{\partial y}{\partial \eta} d\eta \end{Bmatrix} = \left[\begin{Bmatrix} \frac{\partial x}{\partial \xi} \\ \frac{\partial y}{\partial \xi} \end{Bmatrix} \times \begin{Bmatrix} \frac{\partial x}{\partial \eta} \\ \frac{\partial y}{\partial \eta} \end{Bmatrix} \right] d\xi d\eta$$

$$\therefore dA_2 = \left(\frac{\partial x}{\partial \xi} \frac{\partial y}{\partial \eta} - \frac{\partial x}{\partial \eta} \frac{\partial y}{\partial \xi} \right) d\xi d\eta$$

Therefore, to scale from natural to global axes:

$$\frac{dA_2}{dA_1} = \frac{\left(\frac{\partial x}{\partial \xi} \frac{\partial y}{\partial \eta} - \frac{\partial x}{\partial \eta} \frac{\partial y}{\partial \xi} \right) d\xi d\eta}{d\xi \times d\eta} = \left(\frac{\partial x}{\partial \xi} \frac{\partial y}{\partial \eta} - \frac{\partial x}{\partial \eta} \frac{\partial y}{\partial \xi} \right)$$

By convention, this is represented as the determinant of the Jacobian, where the Jacobian is represented as:

$$\boldsymbol{J} = \begin{bmatrix} \frac{dx}{d\xi} & \frac{dx}{d\eta} \\ \frac{dy}{d\xi} & \frac{dy}{d\eta} \end{bmatrix}$$

Therefore, the area can be represented by:

$$dA = dxdy = |\boldsymbol{J}| d\xi d\eta$$

Thus, substituting into (2):

$$\iint \phi(x,y) dA = \int_{-1}^{1} \int_{-1}^{1} \phi(\xi,\eta) \, |\boldsymbol{J}| d\xi \, d\eta \tag{3}$$

Now say the derivative of $\phi(x,y)$ with respect to x or y is required. Applying the multivariable chain rule:

$$\frac{\partial \phi}{\partial \xi} = \frac{\partial \phi}{\partial x} \cdot \frac{\partial x}{\partial \xi} + \frac{\partial \phi}{\partial y} \cdot \frac{\partial y}{\partial \xi}$$
$$\frac{\partial \phi}{\partial \eta} = \frac{\partial \phi}{\partial x} \cdot \frac{\partial x}{\partial \eta} + \frac{\partial \phi}{\partial y} \cdot \frac{\partial y}{\partial \eta}$$

This can be formed into the product of a matrix and a vector of the partial derivatives:

$$\begin{Bmatrix} \frac{\partial \phi}{\partial \xi} \\ \frac{\partial \phi}{\partial \eta} \end{Bmatrix} = \begin{bmatrix} \frac{dx}{d\xi} & \frac{dy}{d\xi} \\ \frac{dx}{d\eta} & \frac{dx}{d\eta} \end{bmatrix} \begin{Bmatrix} \frac{\partial \phi}{\partial x} \\ \frac{\partial \phi}{\partial y} \end{Bmatrix}$$

Notice that the matrix is the transpose of the Jacobian.

$$\therefore \begin{Bmatrix} \frac{\partial \phi}{\partial \xi} \\ \frac{\partial \phi}{\partial \eta} \end{Bmatrix} = \boldsymbol{J}^T \begin{Bmatrix} \frac{\partial \phi}{\partial x} \\ \frac{\partial \phi}{\partial y} \end{Bmatrix}$$

However, $\frac{\partial \phi}{\partial x}$ and $\frac{\partial \phi}{\partial y}$ need to be calculated. Therefore, left multiplying by the inverse of J^T

$$\begin{Bmatrix} \frac{\partial \phi}{\partial x} \\ \frac{\partial \phi}{\partial y} \end{Bmatrix} = (\boldsymbol{J}^T)^{-1} \begin{Bmatrix} \frac{\partial \phi}{\partial \xi} \\ \frac{\partial \phi}{\partial \eta} \end{Bmatrix} \tag{4}$$

Isoparametric Shape Functions

The element property at any point in the isoparametric quad can be represented as a multivariate polynomial with istotropic properties in ξ and η:

$$\phi = \alpha_0 + \alpha_1 \xi + \alpha_2 \eta + \alpha_3 \xi\eta + \alpha_4 \xi^2 + \alpha_5 \eta^2 + \alpha_6 \xi\eta^2 + \alpha_7 \xi^2 \eta$$

Or, in matrix form:

$$\phi = [1 \quad \xi \quad \eta \quad \xi\eta \quad \xi^2 \quad \eta^2 \quad \xi\eta^2 \quad \xi^2\eta] \begin{Bmatrix} \alpha_0 \\ \alpha_1 \\ \alpha_2 \\ \alpha_3 \\ \alpha_4 \\ \alpha_5 \\ \alpha_6 \\ \alpha_7 \end{Bmatrix} \tag{5}$$

However, in FEM, it is preferable to represent this as a linear combination of the nodal values and the shape functions:

$$\phi(x,y) = \phi_1 N_1 + \phi_2 N_2 + \phi_3 N_3 + \phi_4 N_4 + \phi_5 N_5 + \phi_6 N_6 + \phi_7 N_7 + \phi_8 N_8 \tag{6}$$

At node n, the value of $\phi(x,y)$ should be ϕ_n. Thus:

$$N_i = 1 \; \forall \; i = n$$
$$N_i = 0 \; \forall \; i \neq n$$

Let $\boldsymbol{\phi}$ **be** a vector of the nodal values of $\phi(x,y)$:

$$\boldsymbol{\phi} = [\phi_1 \quad \phi_2 \quad \phi_3 \quad \phi_4 \quad \phi_5 \quad \phi_6 \quad \phi_7 \quad \phi_8]^T$$

Using the definition of $\boldsymbol{\phi}$ and (5):

$$\boldsymbol{\phi} = \begin{bmatrix} 1 & \xi_1 & \eta_1 & \xi_1\eta_1 & \xi_1^2 & \eta_1^2 & \xi_1\eta_1^2 & \xi_1^2\eta_1 \\ 1 & \xi_2 & \eta_2 & \xi_2\eta_2 & \xi_2^2 & \eta_2^2 & \xi_2\eta_2^2 & \xi_2^2\eta_2 \\ & & & & \dots & & & \\ 1 & \xi_8 & \eta_8 & \xi_8\eta_8 & \xi_8^2 & \eta_8^2 & \xi_8\eta_8^2 & \xi_8^2\eta_8 \end{bmatrix} \begin{Bmatrix} \alpha_0 \\ \alpha_1 \\ \alpha_2 \\ \alpha_3 \\ \alpha_4 \\ \alpha_5 \\ \alpha_6 \\ \alpha_7 \end{Bmatrix}$$

Where ξ_n and η_n represent the nodal values of ξ and η

Substituting the nodal co-ordinates from Figure 2, the formulation in **Appendix A** is obtained.

The coefficients can then be calculated as:

$$\boldsymbol{\alpha} = \boldsymbol{A^{-1}\phi}$$

Thus:

$$\phi = [1 \quad \xi \quad \eta \quad \xi\eta \quad \xi^2 \quad \eta^2 \quad \xi\eta^2 \quad \xi^2\eta]\boldsymbol{A^{-1}\phi}$$

Expanding this gives the form of (6). Hence, the coefficients of ϕ_i will then be the shape functions. Carrying out this procedure, the shape functions are obtained. These can be found in **Appendix B** along with the code to solve this. The derivatives of these will also be required and are tabulated in **Appendix C**.

3.2. Gaussian Quadrature

The equations resulting from the Finite Element Method will involve integrals, which need to be solved numerically for the chosen element type. One well-known method for numerical integration is the trapezoidal integration rule. It approximates the integral by discretizing the function into a set of trapezoids, expressing the solution as a linear combination of the function evaluated at specific sampling points. While this method is simple and powerful, it is accurate only for linear functions. Consequently, evaluating integrals of high-order polynomials with sufficient accuracy requires many sampling points, which can be computationally inefficient.

Gaussian Quadrature addresses this limitation by enabling the exact solution of integrals involving polynomials of degree $2m-1$ using only m sampling points. Initially, this may seem to contradict the fundamental theorem of algebra, which states that an n-degree polynomial can be uniquely represented with $n+1$ points. However, through the process of orthogonalization, which is employed in the derivation of various algorithms such as the

Fourier transform and later in this paper for the modal reduction technique, this becomes achievable.

Like the trapezoidal method, the Gaussian Quadrature will be formulated as a weighted sum of the function evaluated at sampling points. However, Gaussian Quadrature chooses the sampling points wisely, to allow for greater efficiency. Furthermore, Gaussian Quadrature also differs by approaching the problem with linear algebra, rather than geometry.

To formulate the Gaussian Quadrature technique, a good foundation on several techniques must be made. Firstly, polynomial orthogonality regarding the inner product will be demonstrated. Subsequently, an orthogonal basis set, denoted as L_m, will be constructed from the set of polynomials $[1, x, x^2, \dots]$. It will be shown that L_m is orthogonal to all polynomials of degree m or less. These concepts will then be employed to prove that the integral of a polynomial of degree $2m-1$ can be represented as the integral of a polynomial of degree m, providing insights into where to sample for integration. Finally, the procedure for generating these orthogonal polynomials will be presented.

Polynomial Orthogonality

The inner product will be defined as:

$$\langle p(x), q(x) \rangle = \int_{-1}^{1} p(x) \cdot q(x)\, dx \tag{7}$$

$p(x)$ and $q(x)$ are considered orthogonal with respect to the chosen inner product if:

$$\langle p(x), q(x) \rangle = 0$$

Alternatively, from (7):

$$\langle p(x), q(x) \rangle = \int_{-1}^{1} p(x) \cdot q(x)\, dx = 0 \tag{8}$$

Let $L_m(x)$ represent a polynomial set which forms an orthogonal basis of the polynomial set $[1, x, x^2, \dots]$. It will now be proved that L_m is orthogonal to any polynomial of degree m or less (using a method not derived from any reference).

Since L_m forms an orthogonal basis, any polynomial $q_n(x)$ of degree n can be represented as: $\sum_{i=0}^{n} a_i L_i(x)$. Substituting $L_{n+1}(x)$ and $\sum_{i=0}^{n} a_i L_i(x)$ as p and q into (7):

$$\int_{-1}^{1} L_{n+1}(x) \cdot q_n(x)\, dx = \int_{-1}^{1} L_{n+1}(x) \cdot \sum_{i=0}^{n} a_i L_i(x)\ dx \tag{9}$$

Since L_{n+1} is constant with respect to the sum:

$$\int_{-1}^{1} L_{n+1}(x) \cdot \sum_{i=0}^{n} a_i L_i(x)\ dx = \int_{-1}^{1} \sum_{i=0}^{n} a_i L_i(x) L_{n+1}(x)\ dx$$

Swapping the sum and integral:

$$\int_{-1}^{1} \sum_{i=0}^{n} a_i L_i(x) L_{n+1}(x)\ dx = \sum_{i=0}^{n} \int_{-1}^{1} a_i L_i(x) L_{n+1}(x)$$

Since L_m is an orthogonal basis, L_{n+1} is orthogonal to all L_m where $m \neq n+1$. Therefore:

$$\sum_{i=0}^{n} \int_{-1}^{1} a_i L_i(x) L_{n+1}(x) = 0$$

Recalling the LHS of (9):

$$\int_{-1}^{1} L_{n+1}(x) \cdot q_n(x)\, dx = \sum_{i=0}^{n} \int_{-1}^{1} a_i L_i(x) L_{n+1}(x) = 0$$

This suits the definition of orthogonality with respect to the chosen inner product:

$$\langle L_{n+1}(x), q_n(x) \rangle = \int_{-1}^{1} L_{n+1}(x) \cdot q_n(x)\, dx = 0 \tag{10}$$

Since q_n is any n degree polynomial, this proves that L_{n+1} is orthogonal to any polynomial of degree n or lower.

Reducing Integral Polynomial Degree

It will now be shown that the integral of a polynomial of degree $2m-1$ can be represented with the integral of a polynomial of degree m. This was derived by Gauss.
Let $P_{2m-1}(x)$, represent any polynomial of degree $2m-1$. This can be divided by L_m using polynomial division:

$$P_{2m-1}(x) = Q(x)L_m(x) + R(x) \tag{11}$$

Through rules of polynomial division, $Q(x)$ and $R(x)$ are of degree $m-1$ or lower.
Integrating both sides:

$$\int_{-1}^{1} P_{2m-1}(x)\,dx = \int_{-1}^{1} Q(x)L_m(x)\,dx + \int_{-1}^{1} R(x)\,dx \tag{12}$$

Since $Q(x)$ is a polynomial of degree $m-1$ or lower, (10) applies, thus:

$$\int_{-1}^{1} Q(x)L_m(x)\,dx = 0$$

This is such that (12) can be reduced to:

$$\int_{-1}^{1} P_{2m-1}(x)\,dx = \int_{-1}^{1} R(x)\,dx \tag{13}$$

Recall that $R(x)$ is a $m-1$ or lower degree polynomial. Thus, the integral of a $2m-1$ degree polynomial can be represented as the integral of an m degree polynomial. So, now the function $R(x)$ needs to be obtained. From (11), at the zeros L_m, only $R(x)$ remains. Thus, by sampling the original polynomial at the zeros of L_m (of which there are m), the integral of $R(x)$ can be taken, which is equivalent to the integral of the original polynomial (from (13)). Note that since $R(x)$ is of degree $m-1$ or less, sampling m points will yield correct integration. This reduces the sampling points of the original problem from $2m-1$ to m. The reader may attempt to repeat this procedure to further reduce the required sampling points, but this is not possible.

Generating L_m Polynomials

Now, to generate the L_m from the $[1, x, x^2, \dots]$ set, the Gram-Schmidt procedure will be demonstrated. Vectors will be utilised as a visual aid although this will be applied to polynomials.

Figure 5 and Figure 6 illustrate the process of orthogonalization, where the vectors $\boldsymbol{u}_1$ and $\boldsymbol{u}_2$ are transformed into orthogonal vectors $\boldsymbol{v}_1$ and $\boldsymbol{v}_2$, whist maintaining their general direction.

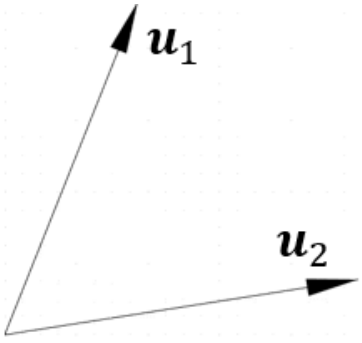

Figure 5: Two vectors $\boldsymbol{u}_1$ and $\boldsymbol{u}_2$ spanning a space

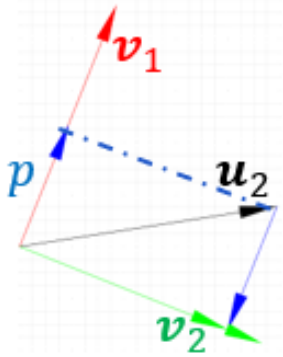

Figure 6: The orthogonalization of the vectors $\boldsymbol{u}_1$ and $\boldsymbol{u}_2$ into $\boldsymbol{v}_1$ and $\boldsymbol{v}_2$

Initially, the vector $\boldsymbol{u}_1$ is chosen as the orthogonal basis, denoted as $\boldsymbol{v}_1$. Then, by subtracting the projection of $\boldsymbol{u}_2$ onto $\boldsymbol{v}_1$ from $\boldsymbol{u}_2$, only the orthogonal component remains. Consequently,

a new orthogonal vector, $\boldsymbol{v}_2$, is generated. This procedure ensures that $\boldsymbol{v}_1$ and $\boldsymbol{v}_2$ are orthogonal to each other.
Mathematically:
Set $\boldsymbol{v}_1 = \boldsymbol{u}_1$
Then, let $\boldsymbol{p}$ be the projection of $\boldsymbol{u}_2$ onto $\boldsymbol{v}_1$:

$$\boldsymbol{p} = \frac{\boldsymbol{v}_1 \cdot \boldsymbol{u}_2}{||\boldsymbol{v}_1||^2}\boldsymbol{v}_1$$

The dot product of a vector with itself is:

$$\boldsymbol{v}_1 \cdot \boldsymbol{v}_1 = ||\boldsymbol{v}_1||^2$$

Thus:

$$\boldsymbol{p} = \frac{\boldsymbol{v}_1 \cdot \boldsymbol{u}_2}{\boldsymbol{v}_1 \cdot \boldsymbol{v}_1}\boldsymbol{v}_1$$

Then, a vector orthogonal to $\boldsymbol{v}_1$ can be found by subtracting p from $\boldsymbol{u}_2$ since only the part orthogonal to $\boldsymbol{v}_1$ will remain.

$$\boldsymbol{v}_2 = \boldsymbol{u}_2 - \boldsymbol{p}$$
$$\therefore \boldsymbol{v}_2 = \boldsymbol{u}_2 - \frac{\boldsymbol{v}_1 \cdot \boldsymbol{u}_2}{\boldsymbol{v}_1 \cdot \boldsymbol{v}_1}\boldsymbol{v}_1$$

As long as there is sufficient dimensionality, this process can be repeated by continuing the process. If not, successive vectors will return 0. In general:

$$\boldsymbol{v}_n = \boldsymbol{u}_n - \frac{\boldsymbol{v}_1 \cdot \boldsymbol{u}_n}{\boldsymbol{v}_1 \cdot \boldsymbol{v}_1}\boldsymbol{v}_1 - \frac{\boldsymbol{v}_2 \cdot \boldsymbol{u}_n}{\boldsymbol{v}_2 \cdot \boldsymbol{v}_2}\boldsymbol{v}_2 - \cdots - \frac{\boldsymbol{v}_{n-1} \cdot \boldsymbol{u}_n}{\boldsymbol{v}_{n-1} \cdot \boldsymbol{v}_{n-1}}\boldsymbol{v}_{n-1}$$
$$\boldsymbol{v}_n = \boldsymbol{u}_n - \sum_{i=1}^{n-1} \frac{\boldsymbol{v}_i \cdot \boldsymbol{u}_n}{\boldsymbol{v}_i \cdot \boldsymbol{v}_i}\boldsymbol{v}_i$$

Generalising this to the inner product:

$$\boldsymbol{v}_n = \boldsymbol{u}_n - \sum_{i=1}^{n-1} \frac{\langle \boldsymbol{v}_i, \boldsymbol{u}_n \rangle}{\langle \boldsymbol{v}_i, \boldsymbol{v}_i \rangle}\boldsymbol{v}_i \tag{14}$$

Throughout the derivation, the inner product was assumed to follow these properties [20]:

1. $\langle u + v, w \rangle = \langle u, w \rangle + \langle v, w \rangle$
2. $\langle \alpha v, w \rangle = \alpha \langle v, w \rangle$
3. $\langle v, w \rangle = \langle w, v \rangle$
4. $\langle v, v \rangle \geq 0$ and equal if and only if $v = 0$

It is simple to test whether the inner product defined in (8) passes these. It in fact does and so the orthogonalization procedure is valid.

Calculating Weights and Gauss Points

From the structural equations, quartic polynomials will be integrated. This requires a bit of insight but can be seen in later sections. Regardless, the derivations are placed here to keep this topic in this section. The integral of an n degree polynomial can be represented as:

$$\int_{-1}^{1} p_n(x)\, dx = \sum_{i=1}^{n} w_i p_n(x_i)\, dx$$

For full integration, the polynomial is of degree 4 and so will require 3x3 integration points using Gaussian Quadrature. Thus, the reduced case will require 2x2 integration points. With Gaussian Quadrature, this corresponds to solving the integrals of quadratic and linear polynomials. Examples of this can be seen in Figure 7 and Figure 8. Hence, reduced integration presents the benefit of 2.25 times less computations exactly.

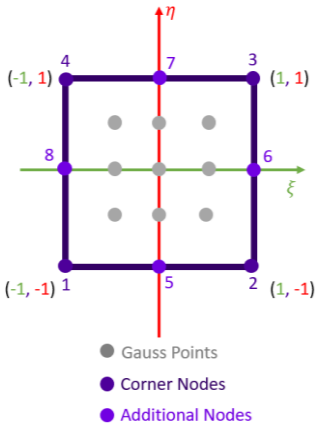

Figure 7: Fully integrated element

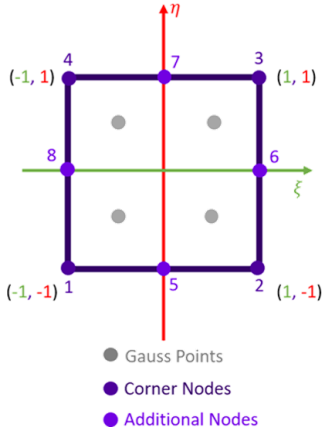

Figure 8: Reduced integrated element

Firstly, the reduced case will be tackled. The derivation of the full integration scheme can be seen in **Appendix D** (although it is not used for this project).
To generate L_m:
The basis for this is up to quadratic:

$$[1, x, x^2]$$

1 is taken as the first basis. Then, the next basis is:

$$x - 1 \cdot \frac{\int_{-1}^{1} 1 \cdot x \, dx}{\int_{-1}^{1} x \cdot x \, dx} = x - 0 = x$$

Then, the next is:

$$x^2 - 1 \cdot \frac{\int_{-1}^{1} 1 \cdot x^2 \, dx}{\int_{-1}^{1} 1 \cdot 1 \, dx} - x \cdot \frac{\int_{-1}^{1} x \cdot x^2 \, dx}{\int_{-1}^{1} x \cdot x \, dx} = x^2 - \frac{1}{3}$$

The orthogonal basis is then:

$$[1, x, x^2 - \frac{1}{3}]$$

The Gauss points are then the roots of L_2: $x^2 - \frac{1}{3} = 0$. Or: $\pm\sqrt{\frac{1}{3}}$.
Since reduced integration considers the integral of a cubic, the reduced integral case will be linear:

$$R_1(x) = a_0 + a_1 x$$

The integral of this is:

$$\int_{-1}^{1} R_1(x) \, dx = \int_{-1}^{1} (a_0 + a_1 x) dx$$

Through the linear property of integrals:

$$\int_{-1}^{1} R_1(x) \, dx = \int_{-1}^{1} a_0 dx + \int_{-1}^{1} a_1 x dx$$

The integral is approximated as the following linear combination:

$$\int_{-1}^{1} R_1(x) \, dx = \sum_{i=1}^{2} w(x_i) R_1(x_i) \tag{15}$$

The closed-form solution is then:

$$\int_{-1}^{1} R_1(x) \, dx = 2a_0 + 0a_1 \tag{16}$$

From (15):

$$\int_{-1}^{1} R_1(x) \, dx = w(x_1) R_1(x_1) + w(x_2) R_1(x_2)$$

Substituting (16):

$$\int_{-1}^{1} R_1(x)\,dx = w(x_1)(a_0 + a_1x_1) + w(x_2)(a_0 + a_1x_2)$$

Factorising:

$$\int_{-1}^{1} R_1(x)\,dx = \big(w(x_1) + w(x_2)\big)a_0 + (w_1x_1 + w_2x_2)a_1 \tag{17}$$

Comparing (16) and (17) and formulating this as a matrix:

$$\begin{bmatrix} 1 & 1 \\ x_1 & x_2 \end{bmatrix}\begin{bmatrix} w_1 \\ w_2 \end{bmatrix} = \begin{bmatrix} 2 \\ 0 \end{bmatrix}$$

Substituting the corresponding Gauss Points for x_1 and x_2:

$$\begin{bmatrix} 1 & 1 \\ \frac{1}{\sqrt{3}} & -\frac{1}{\sqrt{3}} \end{bmatrix}\begin{bmatrix} w_1 \\ w_2 \end{bmatrix} = \begin{bmatrix} 2 \\ 0 \end{bmatrix}$$

Solving for w_1 and w_2:

$$w_1 = 1 \text{ and } w_2 = 1$$

Appendix E summarises the Gauss points and the corresponding weights for both the Full and Reduced case.

3.3. Energy Methods

The total energy of a system is given as a sum of the strain energy, the kinetic energy and the external work. Given that each property is a function of a displacement field $\boldsymbol{d}$:

$$\pi(\boldsymbol{d}) = W(\boldsymbol{d}) - T(\boldsymbol{d}) + U(\boldsymbol{d})$$

where π is the total energy, W is the external work, T is the kinetic energy and U is the strain energy.

The strain energy is given as [4]:

$$U(\boldsymbol{d}) = \frac{1}{2}\iiint \boldsymbol{\epsilon}^T \boldsymbol{Q}\boldsymbol{\epsilon} dV$$

where $\boldsymbol{\epsilon}$ is a function of $\boldsymbol{d}$ and **Q** is the constitutive matrix.

The volume integral can be transformed into integrating along the natural coordinates and along the thickness. With reference to (3):

$$U(\boldsymbol{d}) = \frac{1}{2}\int_{z_1}^{z_2}\int_{-1}^{-1}\int_{-1}^{1} \boldsymbol{\epsilon}^T \boldsymbol{Q}\boldsymbol{\epsilon}\,|\boldsymbol{J}|d\xi d\eta dz \tag{18}$$

Similarly, the work done is given by the product of force and displacement. In integral form:

$$W = \int_{-1}^{-1}\int_{-1}^{1} \Delta p \cdot w\,|\boldsymbol{J}|d\xi d\eta dz \tag{19}$$

The kinetic energy equation $T = \frac{1}{2}m\dot{x}^2$ in integral form is:

$$T = \frac{1}{2}\iiint (\dot{u}^2 + \dot{v}^2 + \dot{w}^2)dV$$

Similarly:

$$T = \frac{1}{2}\int_{z_1}^{z_2}\int_{-1}^{-1}\int_{-1}^{1} (\dot{u}^2 + \dot{v}^2 + \dot{w}^2)\,|\boldsymbol{J}|d\xi d\eta dz \tag{20}$$

Hamilton's Principle states that the total energy functional should be minimised. The proof is out of the scope of this paper; however, it is a property many systems exhibit. To simplify, the displacement field will be assumed to be a multivariate polynomial. Thus, the energy is now a function (rather than a functional) and can be minimised using calculus:

$$\frac{\partial \pi(\boldsymbol{d})}{\partial \boldsymbol{d}} = \frac{\partial U(\boldsymbol{d})}{\partial \boldsymbol{d}} + \frac{\partial W(\boldsymbol{d})}{\partial \boldsymbol{d}} - \frac{\partial T(\boldsymbol{d})}{\partial \boldsymbol{d}} = 0 \tag{21}$$

From (21), the stiffness matrix will be obtained through factoring $\boldsymbol{d}$ from the 1st term. The aerodynamic stiffness matrix will be obtained through factoring $\boldsymbol{d}$ from the 2nd term. Finally,

the mass matrix will be obtained from factoring $\ddot{\boldsymbol{d}}$ from the 3rd term. By performing this, the following form will be obtained for aeroelastic analysis [4]:

$$\boldsymbol{M}\ddot{\boldsymbol{d}} + (\boldsymbol{K} + \lambda \boldsymbol{K}_a)\boldsymbol{d} = 0 \tag{22}$$

Where $\boldsymbol{K}, \boldsymbol{M}$ and $\boldsymbol{K}_a$ are the stiffness, mass and aerodynamic matrices respectively. λ is the pressure parameter which will be explored later.

This can then be solved to return $\boldsymbol{d}$ which minimises total energy, which is how the structure is expected to deform.

Note that the derivative with respect to a vector is as follows:

$$\frac{\partial(\boldsymbol{x}^T \boldsymbol{A}\boldsymbol{x})}{\partial \boldsymbol{x}} = 2\boldsymbol{A}\boldsymbol{x} \tag{23}$$

This will be fundamental to the formulation of the stiffness matrices.

3.4. Reissner-Mindlin Plate Theory

In this section, the constitutive and strain-displacement relationships will be utilised to produce the FEM form of Mindlin plate theory. The structural derivation is modified from, [21], but the FEM formulation is work from this project.

The assumptions for this section will be:

- Straight lines normal to the mid-surface remain straight after deformation [21]
- Straight lines normal to the mid-surface remain normal to the mid-surface after deformation [21]
- The thickness of the plate does not change during a deformation [21]
- Isotropic
- Fibres perpendicular to middle plane of the plate remain straight but can rotate after deformation [21].
- Linear elasticity
- Small deformations

The required material properties are:

- h (thickness)
- E
- ν
- ρ

The plate sign conventions can be seen in Figure 9. These must be adhered to throughout the derivation.

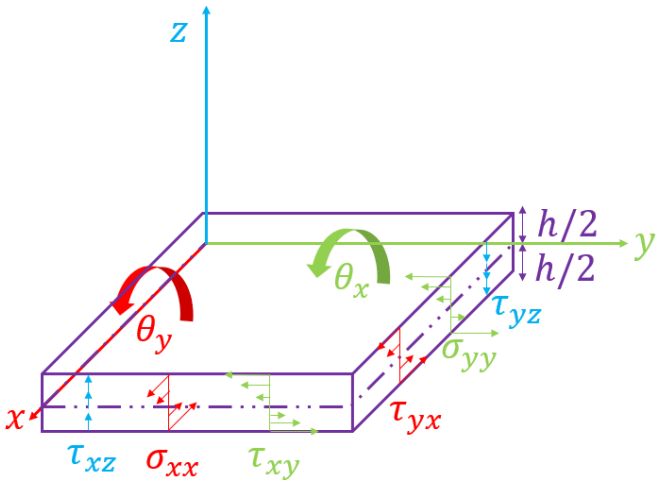

Figure 9: Sign convention for Reissner-Mindlin plate

The displacements of the plate in the x, y and z axes are u, v and w respectively.

From Figure 9, the stress vector can be written:

$$\boldsymbol{\sigma} = \begin{Bmatrix} \sigma_{xx} \\ \sigma_{yy} \\ \tau_{xy} \\ \tau_{xz} \\ \tau_{yz} \end{Bmatrix}$$

Notably, τ_{xz} and τ_{yz} would be neglected in classical plate theory.
Using the small angle assumptions and by referring to Figure 10 and Figure 11 the displacements can be expressed as:

$$u = z\theta_x, v = z\theta_y \tag{24}$$

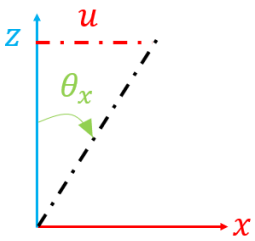

Figure 10: Displacement angle relations θ_x

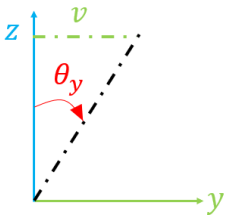

Figure 11: Displacement angle relations θ_y

The strains can then be formulated using the derivatives and substituting (24):

- $\epsilon_{xx} = \frac{\partial u}{\partial x} = z\frac{\partial \theta_x}{\partial x}$
- $\epsilon_{yy} = \frac{\partial v}{\partial y} = z\frac{\partial \theta_y}{\partial y}$
- $\gamma_{xy} = \frac{\partial u}{\partial y} + \frac{\partial v}{\partial x} = z\left(\frac{\partial \theta_y}{\partial x} + \frac{\partial \theta_x}{\partial y}\right)$
- $\gamma_{xz} = \frac{\partial u}{\partial z} + \frac{\partial w}{\partial x} = \theta_x + \frac{\partial w}{\partial x}$
- $\gamma_{yz} = \frac{\partial v}{\partial z} + \frac{\partial w}{\partial y} = \theta_y + \frac{\partial w}{\partial y}$

From these strains, the degrees of freedom are w, θ_x and θ_y. With this, they can be approximated using the shape functions in matrix form:

$$\begin{Bmatrix} w \\ \theta_x \\ \theta_y \end{Bmatrix} = \begin{pmatrix} N_1 & 0 & 0 & N_2 & 0 & 0 & \dots & N_8 & 0 & 0 \\ 0 & N_1 & 0 & 0 & N_2 & 0 & \dots & 0 & N_8 & 0 \\ 0 & 0 & N_1 & 0 & 0 & N_2 & \dots & 0 & 0 & N_8 \end{pmatrix} \begin{Bmatrix} w_1 \\ \theta_{x1} \\ \theta_{y2} \\ w_2 \\ \theta_{x2} \\ \theta_{y2} \\ \dots \\ w_8 \\ \theta_{x8} \\ \theta_{y8} \end{Bmatrix} \tag{25}$$

$$\mathbf{N} \qquad \mathbf{d}$$

Combining the required degrees of freedoms and their derivatives into vector form:

$$\begin{Bmatrix} w \\ \theta_x \\ \theta_y \\ \frac{\partial w}{\partial \xi} \\ \frac{\partial w}{\partial \eta} \\ \frac{\partial \theta_x}{\partial \xi} \\ \frac{\partial \theta_x}{\partial \eta} \\ \frac{\partial \theta_y}{\partial \xi} \\ \frac{\partial \theta_y}{\partial \eta} \end{Bmatrix} = \underbrace{\begin{pmatrix} N_1 & 0 & 0 & N_2 & 0 & 0 & \dots & N_8 & 0 & 0 \\ 0 & N_1 & 0 & 0 & N_2 & 0 & \dots & 0 & N_8 & 0 \\ 0 & 0 & N_1 & 0 & 0 & N_2 & \dots & 0 & 0 & N_8 \\ \frac{\partial N_1}{\partial \xi} & 0 & 0 & \frac{\partial N_2}{\partial \xi} & 0 & 0 & \dots & \frac{\partial N_8}{\partial \xi} & 0 & 0 \\ \frac{\partial N_1}{\partial \eta} & 0 & 0 & \frac{\partial N_2}{\partial \eta} & 0 & 0 & \dots & \frac{\partial N_8}{\partial \eta} & 0 & 0 \\ 0 & \frac{\partial N_1}{\partial \xi} & 0 & 0 & \frac{\partial N_2}{\partial \xi} & 0 & \dots & 0 & \frac{\partial N_8}{\partial \xi} & 0 \\ 0 & \frac{\partial N_1}{\partial \eta} & 0 & 0 & \frac{\partial N_2}{\partial \eta} & 0 & \dots & 0 & \frac{\partial N_8}{\partial \eta} & 0 \\ 0 & 0 & \frac{\partial N_1}{\partial \xi} & 0 & 0 & \frac{\partial N_2}{\partial \xi} & \dots & 0 & 0 & \frac{\partial N_8}{\partial \xi} \\ 0 & 0 & \frac{\partial N_1}{\partial \eta} & 0 & 0 & \frac{\partial N_2}{\partial \eta} & \dots & 0 & 0 & \frac{\partial N_8}{\partial \eta} \end{pmatrix}}_{\boldsymbol{\delta}} \boldsymbol{d} \tag{26}$$

Using (4):

$$\begin{Bmatrix} w \\ \theta_x \\ \theta_y \\ \frac{\partial w}{\partial x} \\ \frac{\partial w}{\partial y} \\ \frac{\partial \theta_x}{\partial x} \\ \frac{\partial \theta_x}{\partial y} \\ \frac{\partial \theta_y}{\partial x} \\ \frac{\partial \theta_y}{\partial y} \end{Bmatrix} = \underbrace{\begin{pmatrix} 1 & 0 & 0 & \mathbf{0} & \mathbf{0} & \mathbf{0} \\ 0 & 1 & 0 & \mathbf{0} & \mathbf{0} & \mathbf{0} \\ 0 & 0 & 1 & \mathbf{0} & \mathbf{0} & \mathbf{0} \\ \mathbf{0} & \mathbf{0} & \mathbf{0} & (\boldsymbol{J}^T)^{-1} & \mathbf{0} & \mathbf{0} \\ \mathbf{0} & \mathbf{0} & \mathbf{0} & \mathbf{0} & (\boldsymbol{J}^T)^{-1} & \mathbf{0} \\ \mathbf{0} & \mathbf{0} & \mathbf{0} & \mathbf{0} & \mathbf{0} & (\boldsymbol{J}^T)^{-1} \end{pmatrix}}_{\boldsymbol{T}} \underbrace{\begin{Bmatrix} w \\ \theta_x \\ \theta_y \\ \frac{\partial w}{\partial \xi} \\ \frac{\partial w}{\partial \eta} \\ \frac{\partial \theta_x}{\partial \xi} \\ \frac{\partial \theta_x}{\partial \eta} \\ \frac{\partial \theta_y}{\partial \xi} \\ \frac{\partial \theta_y}{\partial \eta} \end{Bmatrix}}_{\boldsymbol{\delta d}} \tag{27}$$

From the plane-stress constitutive relations:

$$\underbrace{\begin{Bmatrix} \sigma_{xx} \\ \sigma_{yy} \\ \tau_{xy} \end{Bmatrix}}_{\boldsymbol{\sigma}_1} = \underbrace{\begin{bmatrix} \frac{E}{1-\nu^2} & \frac{E\nu}{1-\nu^2} & 0 \\ \frac{E\nu}{1-\nu^2} & \frac{E}{1-\nu^2} & 0 \\ 0 & 0 & G \end{bmatrix}}_{\boldsymbol{Q}_1} \underbrace{\begin{Bmatrix} \epsilon_{xx} \\ \epsilon_{yy} \\ \gamma_{xy} \end{Bmatrix}}_{\boldsymbol{\epsilon}_1} \tag{28}$$

$$\underbrace{\begin{Bmatrix} \tau_{xz} \\ \tau_{yz} \end{Bmatrix}}_{\boldsymbol{\sigma}_2} = \underbrace{\begin{bmatrix} kG & 0 \\ 0 & kG \end{bmatrix}}_{\boldsymbol{Q}_2} \underbrace{\begin{Bmatrix} \gamma_{xz} \\ \gamma_{yz} \end{Bmatrix}}_{\boldsymbol{\epsilon}_2} \tag{29}$$

Where k is the shear stress correction factor ($5/6$ for this project [4]*)*

Formulating the strain relations in vector format:

$$\boldsymbol{\epsilon_1} = \begin{Bmatrix}\epsilon_{xx}\\ \epsilon_{yy}\\ \gamma_{xy}\end{Bmatrix} = z\begin{bmatrix}0&0&0&0&0&1&0&0&0\\ 0&0&0&0&0&0&0&0&1\\ 0&0&0&0&0&0&1&1&0\end{bmatrix}\begin{Bmatrix} w\\ \theta_x\\ \theta_y\\ \frac{\partial w}{\partial x}\\ \frac{\partial w}{\partial y}\\ \frac{\partial \theta_x}{\partial x}\\ \frac{\partial \theta_x}{\partial y}\\ \frac{\partial \theta_y}{\partial x}\\ \frac{\partial \theta_y}{\partial y}\end{Bmatrix}$$

From (27):

$$\boldsymbol{\epsilon_1} = \begin{Bmatrix}\epsilon_{xx}\\ \epsilon_{yy}\\ \gamma_{xy}\end{Bmatrix} = z\underbrace{\begin{bmatrix}0&0&0&0&0&1&0&0&0\\ 0&0&0&0&0&0&0&0&1\\ 0&0&0&0&0&0&1&1&0\end{bmatrix}}_{\boldsymbol{B_1}}\boldsymbol{T\delta d} \tag{30}$$

Similarly, for $\boldsymbol{\epsilon_2}$:

$$\boldsymbol{\epsilon_2} = \begin{Bmatrix}\gamma_{xz}\\ \gamma_{yz}\end{Bmatrix} = \underbrace{\begin{bmatrix}0&1&0&1&0&0&0&0&0\\ 0&0&1&0&1&0&0&0&0\end{bmatrix}}_{\boldsymbol{B_2}}\boldsymbol{T\delta d} \tag{31}$$

Substituting $\boldsymbol{\epsilon_1}$ and $\boldsymbol{\epsilon_2}$ into (18) and setting the integration limits $z_1 = -\frac{h}{2}$ and $z_2 = \frac{h}{2}$:

$$U(\boldsymbol{d}) = \frac{1}{2}\int_{-\frac{h}{2}}^{\frac{h}{2}}\int_{-1}^{1}\int_{-1}^{1}(\boldsymbol{\epsilon_1^T Q_1 \epsilon_1} + \boldsymbol{\epsilon_2^T Q_2 \epsilon_2})\,|\boldsymbol{J}|d\xi d\eta dz$$

Then, substituting (30) and (31):

$$U(\boldsymbol{d}) = \frac{1}{2}\int_{-\frac{h}{2}}^{\frac{h}{2}}\int_{-1}^{1}\int_{-1}^{1}\left((z\boldsymbol{B_1 T\delta d})^T\boldsymbol{Q_1}(z\boldsymbol{B_1 T\delta d}) + (\boldsymbol{B_2 T\delta d})^T\boldsymbol{Q_2}(\boldsymbol{B_2 T\delta d})\right)|\boldsymbol{J}|d\xi d\eta dz$$

Rearranging (note that the nodal displacements are constant with respect to the integral):

$$U(\boldsymbol{d}) = \frac{1}{2}\boldsymbol{d^T}\int_{-\frac{h}{2}}^{\frac{h}{2}}\int_{-1}^{1}\int_{-1}^{1}\left(z^2(\boldsymbol{B_1 T\delta})^T\boldsymbol{Q_1}(z\boldsymbol{B_1 T\delta})\right)|\boldsymbol{J}|d\xi d\eta dz\,\boldsymbol{d} + \frac{1}{2}\boldsymbol{d^T}\int_{-\frac{h}{2}}^{\frac{h}{2}}\int_{-1}^{1}\int_{-1}^{1}\left((\boldsymbol{B_2 T\delta d})^T\boldsymbol{Q_2}(\boldsymbol{B_2 T\delta d})\right)|\boldsymbol{J}|d\xi d\eta dz\,\boldsymbol{d}$$

Since strain energy is assumed constant throughout the thickness (h).

$$U(\boldsymbol{d}) = \frac{1}{24}h^3\boldsymbol{d^T}\int_{-1}^{1}\int_{-1}^{1}(\boldsymbol{B_1 T\delta})^T\boldsymbol{Q_1}(z\boldsymbol{B_1 T\delta})|\boldsymbol{J}|\,d\xi d\eta\,\boldsymbol{d} + \frac{1}{2}h\boldsymbol{d^T}\int_{-1}^{1}\int_{-1}^{1}(\boldsymbol{B_2 T\delta d})^T\boldsymbol{Q_2}(\boldsymbol{B_2 T\delta d})|\boldsymbol{J}|\,d\xi d\eta\,\boldsymbol{d}$$

Minimising using (23):

$$\frac{\partial U(\boldsymbol{d})}{\partial \boldsymbol{d}} = \frac{1}{12}h^3\int_{-1}^{1}\int_{-1}^{1}(\boldsymbol{B_1 T\delta})^T\boldsymbol{Q_1}(z\boldsymbol{B_1 T\delta})\,|\boldsymbol{J}|\,d\xi d\eta\,\boldsymbol{d} + h\int_{-1}^{1}\int_{-1}^{1}(\boldsymbol{B_2 T\delta d})^T\boldsymbol{Q_2}(\boldsymbol{B_2 T\delta d})\,|\boldsymbol{J}|\,d\xi d\eta\,\boldsymbol{d} = 0$$

Thus, the stiffness matrix can be calculated through factoring $\boldsymbol{d}$ as in (22):

$$\boldsymbol{K}_{Mindlin} = \frac{h^3}{12}\int_{-1}^{1}\int_{-1}^{1}(\boldsymbol{B}_1\boldsymbol{T}\boldsymbol{\delta})^T\boldsymbol{Q}_1(z\boldsymbol{B}_1\boldsymbol{T}\boldsymbol{\delta})|\boldsymbol{J}|\,d\xi d\eta + h\int_{-1}^{1}\int_{-1}^{1}\int_{-1}^{1}(\boldsymbol{B}_2\boldsymbol{T}\boldsymbol{\delta}\boldsymbol{d})^T\boldsymbol{Q}_2(\boldsymbol{B}_2\boldsymbol{T}\boldsymbol{\delta}\boldsymbol{d})\,|\boldsymbol{J}|\,d\xi d\eta \quad (32)$$

Now, to find the mass matrix, the time derivatives of the displacement assumptions will be required:

$$\begin{aligned}\dot{u}(x,y,z,t) &= z\dot{\theta}_x\\ \dot{v}(x,y,z,t) &= z\dot{\theta}_y\\ \dot{w}(x,y,z,t) &= \dot{w}_0\end{aligned}$$

From (20):

$$T = \frac{1}{2}\int_{-\frac{h}{2}}^{\frac{h}{2}}\int_{-1}^{1}\int_{-1}^{1}\rho\left(\left(z\dot{\theta}_x\right)^2+\left(z\dot{\theta}_y\right)^2+\dot{w}_0^2\right)|\boldsymbol{J}|d\xi d\eta dz$$

u_0, v_0, w_0, θ_x and θ_y are the midplane degrees of freedom and so do not vary along the thickness. Thus:

$$T = \frac{1}{2}\int_{-1}^{1}\int_{-1}^{1}\rho\left(\frac{h^3}{12}\dot{\theta_x}^2+\frac{h^3}{12}\dot{\theta_y}^2+h\dot{w}_0^2\right)|\boldsymbol{J}|d\xi d\eta$$

Putting this in matrix form:

$$T = \frac{1}{2}\int_{-1}^{1}\int_{-1}^{1}\begin{Bmatrix}\dot{w}\\ \dot{\theta}_x\\ \dot{\theta}_y\end{Bmatrix}^T\boldsymbol{I}\begin{Bmatrix}\dot{w}\\ \dot{\theta}_x\\ \dot{\theta}_y\end{Bmatrix}|J|d\xi d\eta$$

Where $\boldsymbol{I}$ is the inertial matrix:

$$\boldsymbol{I} = \rho\begin{bmatrix}h & 0 & 0\\ 0 & \frac{h^3}{12} & 0\\ 0 & 0 & \frac{h^3}{12}\end{bmatrix} \quad (33)$$

Note that from (25):

$$\begin{Bmatrix}\dot{w}\\ \dot{\theta}_x\\ \dot{\theta}_y\end{Bmatrix} = \boldsymbol{N}\begin{Bmatrix}\dot{w}_1\\ \dot{\theta}_{x1}\\ \dot{\theta}_{y1}\\ \cdots\\ \dot{w}_8\\ \dot{\theta}_{x8}\\ \dot{\theta}_{y8}\end{Bmatrix} = \boldsymbol{N}\dot{\boldsymbol{d}}$$

$$T = \frac{1}{2}\int_{-1}^{1}\int_{-1}^{1}(\boldsymbol{N}\dot{\boldsymbol{d}})^T\boldsymbol{I}\boldsymbol{N}\dot{\boldsymbol{d}}|J|d\xi d\eta = \frac{1}{2}\int_{-1}^{1}\int_{-1}^{1}\dot{\boldsymbol{d}}^T\boldsymbol{N}^T\boldsymbol{I}\boldsymbol{N}\dot{\boldsymbol{d}}|J|d\xi d\eta$$

$$\frac{\partial T}{\partial\dot{\boldsymbol{d}}} = \int_{-1}^{1}\int_{-1}^{1}\boldsymbol{N}^T\boldsymbol{I}\boldsymbol{N}\dot{\boldsymbol{d}}|J|d\xi d\eta$$

Factoring $\dot{\boldsymbol{d}}$, the mass matrix is:

$$\boldsymbol{M}_{Mindlin} = \int_{-1}^{1}\int_{-1}^{1}\boldsymbol{N}^T\boldsymbol{I}\boldsymbol{N}|J|d\xi d\eta \quad (34)$$

3.5. First Order Shear Deformation Theory (FSDT)

This solution procedure is similar to Mindlin theory and so will be less thorough. If the reader is lost, they are advised to refer to the Mindlin theory section. The sign convention is as Figure 9.

The structural derivations will be from [22]. But the FEM formulation of these will be work from this project.

The assumptions will be:

- Straight lines normal to the mid-surface remain straight after deformation [21]
- Straight lines normal to the mid-surface remain normal to the mid-surface after deformation [21]
- The thickness of the plate does not change during a deformation [21]
- Orthotropic
- Fibres perpendicular to middle plane of the plate remain straight, but can rotate after deformation [21]
- Linear elasticity
- Small deformations

The material properties required are:

- E_L
- E_T
- ν_{LT}
- G_{LT}
- G_{TT}
- Number of layers
- Thickness of each layer
- ρ

The stress-strain relationship is [22]:

$$\begin{Bmatrix}\sigma_{11}\\ \sigma_{21}\\ \tau_{23}\\ \tau_{31}\\ \tau_{12}\end{Bmatrix} = \begin{bmatrix}\bar{Q}_{11} & \bar{Q}_{21} & 0 & 0 & 0\\ \bar{Q}_{21} & \bar{Q}_{22} & 0 & 0 & 0\\ 0 & 0 & \bar{Q}_{44} & 0 & 0\\ 0 & 0 & 0 & \bar{Q}_{55} & 0\\ 0 & 0 & 0 & 0 & \bar{Q}_{66}\end{bmatrix}\begin{Bmatrix}\epsilon_x\\ \epsilon_y\\ \gamma_{yz}\\ \gamma_{xz}\\ \gamma_{xy}\end{Bmatrix}$$

Table 2: $\bar{Q}$ Values

$\bar{Q}_{11} = E_L/(1-\nu_{LT}\nu_{TL})$	$\bar{Q}_{22} = E_T/(1-\nu_{LT}\nu_{TL})$
$\bar{Q}_{22} = E_T/(1-\nu_{LT}\nu_{TL})$	$\bar{Q}_{12} = \nu_{TL}E_L/(1-\nu_{LT}\nu_{TL})$
$\bar{Q}_{21} = \bar{Q}_{12}$	$\bar{Q}_{44} = G_{TT}$
$\bar{Q}_{55} = G_{LT}$	$\bar{Q}_{66} = G_{LT}$

But each laminate can be angled θ around the z axis. Thus, a stress transformation must be made from the laminate axes to the global axes [22]:

$$\begin{Bmatrix}\sigma_x\\ \sigma_y\\ \tau_{yz}\\ \tau_{xz}\\ \tau_{xy}\end{Bmatrix} = \begin{bmatrix}Q_{11} & Q_{12} & 0 & 0 & Q_{16}\\ Q_{21} & Q_{22} & 0 & 0 & Q_{26}\\ 0 & 0 & Q_{44} & Q_{45} & 0\\ 0 & 0 & Q_{45} & Q_{55} & 0\\ Q_{16} & Q_{26} & 0 & 0 & Q_{66}\end{bmatrix}\begin{Bmatrix}\epsilon_x\\ \epsilon_y\\ \gamma_{yz}\\ \gamma_{xz}\\ \gamma_{xy}\end{Bmatrix} \quad (35)$$

The equations of Q are given in Table 3:

Table 3: Q Values

$Q_{11} = U_1 + U_2\cos(2\theta) + U_3\cos(4\theta)$	$Q_{22} = U_1 - U_2\cos(2\theta) + U_3\cos(4\theta)$
$Q_{12} = U_4 - U_3\cos(4\theta)$	$Q_{66} = U_5 - U_3\cos(4\theta)$
$Q_{16} = -\frac{1}{2}U_2\sin(2\theta) - U_3\sin(4\theta)$	$Q_{26} = -\frac{1}{2}U_2\sin(2\theta) - U_3\sin(4\theta)$
$Q_{44} = U_6 + U_7\cos(2\theta)$	$Q_{55} = U_6 - U_7\cos(2\theta)$
$Q_{45} = -U_7\cos(2\theta)$	

The U values are given in Table 4:

Table 4: U Values

$U_1 = \frac{1}{8}(3\bar{Q}_{11} + 3\bar{Q}_{22} + 2\bar{Q}_{12} + 4\bar{Q}_{66})$	$U_2 = \frac{1}{2}(\bar{Q}_{11} - 2\bar{Q}_{22})$
$U_3 = \frac{1}{8}(\bar{Q}_{11} + \bar{Q}_{22} - 2\bar{Q}_{12} - 4\,\bar{Q}_{66})$	$U_4 = \frac{1}{8}(\bar{Q}_{11} + \bar{Q}_{22} + 6\bar{Q}_{12} - 4\bar{Q}_{66})$
$U_5 = \frac{1}{8}(\bar{Q}_{11} + \bar{Q}_{22} - 2\bar{Q}_{12} + 4\bar{Q}_{66})$	$U_6 = \frac{1}{2}(\bar{Q}_{44} + \bar{Q}_{55})$
$U_7 = \frac{1}{2}(\bar{Q}_{44} - \bar{Q}_{55})$	

The strain energy is then:

$$U = \frac{1}{2}\int_{-1}^{-1}\int_{-1}^{1} \boldsymbol{\epsilon}^{*T} \begin{bmatrix} \boldsymbol{A} & \boldsymbol{B} & \boldsymbol{0} \\ \boldsymbol{B} & \boldsymbol{D} & \boldsymbol{0} \\ \boldsymbol{0} & \boldsymbol{0} & \boldsymbol{A_s} \end{bmatrix} \boldsymbol{\epsilon}^{*}\, d\xi d\eta \tag{36}$$

Where:

$$\begin{bmatrix} \boldsymbol{A} & \boldsymbol{B} & \boldsymbol{0} \\ \boldsymbol{B} & \boldsymbol{D} & \boldsymbol{0} \\ \boldsymbol{0} & \boldsymbol{0} & \boldsymbol{A_s} \end{bmatrix} = \begin{bmatrix} A_{11} & & & & & & & \\ A_{12} & A_{22} & & & & & & \\ A_{16} & A_{26} & A_{66} & & & & & \\ B_{11} & B_{12} & B_{16} & D_{11} & Symmetric & & & \\ B_{12} & B_{22} & B_{26} & D_{12} & D_{22} & & & \\ B_{16} & B_{26} & B_{66} & D_{16} & D_{26} & D_{66} & & \\ 0 & 0 & 0 & 0 & 0 & 0 & A_{55} & A_{45} \\ 0 & 0 & 0 & 0 & 0 & 0 & A_{45} & A_{44} \end{bmatrix} \tag{37}$$

The matrix values are given by:

$$(A_{ij}, B_{ij}, D_{ij}) = \int_{-\frac{h}{2}}^{\frac{h}{2}} Q_{ij}(1, z, z^2)dz \;\; i,j = 1,2,6 \tag{38}$$

$$A_{ij} = k^2 \int_{-\frac{h}{2}}^{\frac{h}{2}} Q_{ij}\, dz \;\; i,j = 4,5 \qquad \textit{where } k = \tfrac{5}{6}\,[4] \tag{39}$$

$$\boldsymbol{\epsilon}^{*} = \begin{Bmatrix} \dfrac{\partial u}{\partial x} \\ \dfrac{\partial v}{\partial y} \\ \dfrac{\partial u}{\partial y} + \dfrac{\partial v}{\partial x} \\ \dfrac{\partial w}{\partial y} + \theta_y \\ \dfrac{\partial w}{\partial x} + \theta_x \end{Bmatrix} \tag{40}$$

From $\boldsymbol{\epsilon}^{*}$, the degrees of freedom are u, v, w, θ_x and θ_y (the u and v dofs are additional to the Reissner-Mindlin dofs).

$$\begin{Bmatrix} u \\ v \\ w \\ \theta_x \\ \theta_y \end{Bmatrix} = \begin{pmatrix} N_1 & 0 & 0 & 0 & 0 & \dots & N_8 & 0 & 0 & 0 & 0 \\ 0 & N_1 & 0 & 0 & 0 & \dots & 0 & N_8 & 0 & 0 & 0 \\ 0 & 0 & N_1 & 0 & 0 & \dots & 0 & 0 & N_8 & 0 & 0 \\ 0 & 0 & 0 & N_1 & 0 & \dots & 0 & 0 & 0 & N_8 & 0 \\ 0 & 0 & 0 & 0 & N_1 & \dots & 0 & 0 & 0 & 0 & N_8 \end{pmatrix} \begin{Bmatrix} u_1 \\ v_1 \\ w_1 \\ \theta_{x1} \\ \theta_{y1} \\ \dots \\ u_8 \\ v_8 \\ w_8 \\ \theta_{x8} \\ \theta_{y8} \end{Bmatrix}$$

$$\mathbf{N} \qquad\qquad \mathbf{d}$$

$$\begin{Bmatrix} \theta_x \\ \theta_y \\ \frac{\partial u}{\partial \xi} \\ \frac{\partial u}{\partial \eta} \\ \frac{\partial v}{\partial \xi} \\ \frac{\partial v}{\partial \eta} \\ \frac{\partial w}{\partial \xi} \\ \frac{\partial w}{\partial \eta} \end{Bmatrix} = \begin{pmatrix} 0 & 0 & 0 & N_1 & 0 & \dots & 0 & 0 & 0 & N_8 & 0 \\ 0 & 0 & 0 & 0 & N_1 & \dots & 0 & 0 & 0 & 0 & N_8 \\ \frac{\partial N_1}{\partial \xi} & 0 & 0 & 0 & 0 & \dots & \frac{\partial N_8}{\partial \xi} & 0 & 0 & 0 & 0 \\ \frac{\partial N_1}{\partial \eta} & 0 & 0 & 0 & 0 & \dots & \frac{\partial N_8}{\partial \eta} & 0 & 0 & 0 & 0 \\ 0 & \frac{\partial N_1}{\partial \xi} & 0 & 0 & 0 & \dots & 0 & \frac{\partial N_8}{\partial \xi} & 0 & 0 & 0 \\ 0 & \frac{\partial N_1}{\partial \eta} & 0 & 0 & 0 & \dots & 0 & \frac{\partial N_8}{\partial \eta} & 0 & 0 & 0 \\ 0 & 0 & \frac{\partial N_1}{\partial \xi} & 0 & 0 & \dots & 0 & 0 & \frac{\partial N_8}{\partial \xi} & 0 & 0 \\ 0 & 0 & \frac{\partial N_1}{\partial \eta} & 0 & 0 & \dots & 0 & 0 & \frac{\partial N_8}{\partial \eta} & 0 & 0 \end{pmatrix} \boldsymbol{d}$$

$$\boldsymbol{\delta}$$

$$\begin{Bmatrix} \theta_x \\ \theta_y \\ \frac{\partial u}{\partial x} \\ \frac{\partial u}{\partial y} \\ \frac{\partial v}{\partial x} \\ \frac{\partial v}{\partial y} \\ \frac{\partial w}{\partial x} \\ \frac{\partial w}{\partial y} \end{Bmatrix} = \begin{pmatrix} 1 & 0 & \mathbf{0} & \mathbf{0} & \mathbf{0} \\ 0 & 1 & \mathbf{0} & \mathbf{0} & \mathbf{0} \\ \mathbf{0} & \mathbf{0} & (\boldsymbol{J}^T)^{-1} & \mathbf{0} & \mathbf{0} \\ \mathbf{0} & \mathbf{0} & \mathbf{0} & (\boldsymbol{J}^T)^{-1} & \mathbf{0} \\ \mathbf{0} & \mathbf{0} & \mathbf{0} & \mathbf{0} & (\boldsymbol{J}^T)^{-1} \end{pmatrix} \begin{Bmatrix} \theta_x \\ \theta_y \\ \frac{\partial u}{\partial \xi} \\ \frac{\partial u}{\partial \eta} \\ \frac{\partial v}{\partial \xi} \\ \frac{\partial v}{\partial \eta} \\ \frac{\partial w}{\partial \xi} \\ \frac{\partial w}{\partial \eta} \end{Bmatrix} \tag{41}$$

$$\boldsymbol{T} \qquad\qquad \boldsymbol{\delta d}$$

$$\therefore \boldsymbol{\epsilon}^* = \begin{bmatrix} 0 & 0 & 1 & 0 & 0 & 0 & 0 & 0 \\ 0 & 0 & 0 & 0 & 0 & 1 & 0 & 0 \\ 0 & 0 & 0 & 1 & 1 & 0 & 0 & 0 \\ 0 & 1 & 0 & 0 & 0 & 0 & 0 & 1 \\ 1 & 0 & 0 & 0 & 0 & 0 & 1 & 0 \end{bmatrix} \boldsymbol{T\delta d} \tag{42}$$

$$\mathbf{B}$$

Substituting (42) into (36) and factoring $\boldsymbol{d}$:

$$U = \frac{1}{2}\boldsymbol{d}^T \int_{-1}^{-1} \int_{-1}^{1} (\boldsymbol{BT\delta})^T \begin{bmatrix} \boldsymbol{A} & \boldsymbol{B} & \mathbf{0} \\ \boldsymbol{B} & \boldsymbol{D} & \mathbf{0} \\ \mathbf{0} & \mathbf{0} & \boldsymbol{A_s} \end{bmatrix} \boldsymbol{BT\delta}|\boldsymbol{J}|\, d\xi d\eta\, \boldsymbol{d}$$

Minimising and factoring **d**:

$$\boldsymbol{K}_{FSDT} = \int_{-1}^{-1}\int_{-1}^{1} (\boldsymbol{BT\delta})^T \begin{bmatrix} \boldsymbol{A} & \boldsymbol{B} & \boldsymbol{0} \\ \boldsymbol{B} & \boldsymbol{D} & \boldsymbol{0} \\ \boldsymbol{0} & \boldsymbol{0} & \boldsymbol{A_s} \end{bmatrix} \boldsymbol{BT\delta}|\boldsymbol{J}|\, d\xi d\eta \tag{43}$$

[4] gives the kinetic energy formulation as:

$$T = \frac{1}{2}\int_{-1}^{1}\int_{-1}^{1} \rho h \left(\dot{u}^2 + \dot{v}^2 + \dot{w}^2 + \frac{h^2}{12}\left(\dot{\theta_x}^2 + \dot{\theta_y}^2 \right) \right) |\boldsymbol{J}|\, d\xi d\eta$$

Repeating the same procedure as the Mindlin method, (34):

$$\boldsymbol{M}_{FSDT} = \int_{-1}^{1}\int_{-1}^{1} \boldsymbol{N}^T \boldsymbol{I} \boldsymbol{N} |\boldsymbol{J}| d\xi d\eta \tag{44}$$

But $\boldsymbol{I}$ is now:

$$\boldsymbol{I} = \rho \begin{bmatrix} h & 0 & 0 & 0 & 0 \\ 0 & h & 0 & 0 & 0 \\ 0 & 0 & h & 0 & 0 \\ 0 & 0 & 0 & \frac{h^3}{12} & 0 \\ 0 & 0 & 0 & 0 & \frac{h^3}{12} \end{bmatrix} \tag{45}$$

3.6. Boundary Conditions & Sparse Matrix Approach

Table 5 and Table 6 indicate the boundary conditions for the isotropic and laminate plates respectively. A value of 0 signifies that the degree of freedom (DOF) is constrained to zero, whilst the term “free” indicates that the DOF will be solved for. Since this project will solely tackle rectangular plates, SSSS will indicate simply supported on every outer edge, whilst CCCC will indicate clamped on every outer edge.

Table 5: Isotropic boundary conditions

Isotropic Plate			
	$\boldsymbol{w}$	$\boldsymbol{\theta_x}$	$\boldsymbol{\theta_y}$
Simply Supported	0	free	free
Clamped	0	0	0

Table 6: Laminate boundary conditions

Laminate Plate						
	$\boldsymbol{u}$	$\boldsymbol{v}$	$\boldsymbol{w}$	$\boldsymbol{\theta_x}$	$\boldsymbol{\theta_y}$	$\boldsymbol{\theta_z}$
Simply Supported	0	0	0	free	free	free
Clamped	0	0	0	0	0	0

To handle the 0 boundary conditions, row and column reduction was chosen since it was easier to be more implement over the penalty stiffness method. Additionally, considering that the global stiffness matrix represents direct connections between nodes, the matrix size is proportional to the square of the total number of degrees of freedom. This leads to significant memory and computational demands. However, it is important to note that most matrix entries are zero. By employing a sparse matrix format, only the non-zero elements and their positions are stored, thereby reducing computational requirements.

In contrast to the approach of removing the rows and columns associated with 0 boundary conditions after assembling the global stiffness matrix, a more efficient strategy was employed. The elimination of these rows and columns was performed prior to assembly, thereby reducing memory shifts. This approach ensures that the resulting matrices are more manageable, making the FEM analysis more feasible and resource efficient.

Now, it will be shown how to apply zero boundary conditions to the sparse matrix. This derivation assumes that the matrices are indexed starting at 1. For example, Figure 12 demonstrates a general matrix. Figure 13 is this matrix after the deletion procedure. The red rows and columns in Figure 12 represent the rows and columns to be deleted. In this case, dofs 2 and 4 are to removed. This procedure skips generating the matrix in Figure 12 by directly generating that in Figure 13. This reduces the total number of computational operations, thereby improving efficiency.

DOFs	1	2	3	4	5	…
1						
2						
3						
4						
5						
…						

Figure 12: Full matrix

DOFs	1=>1	3=>2	5=>4	…
1=>1				
3=>2				
5=>4				
…				

Figure 13: Matrix with zero boundary conditions removed

Let S represent an ascendingly ordered set of boundary conditions, where each value represents the dof to be removed. Let i represent an index from the original matrix, and j the index in the reduced matrix. A mapping from i to j is desired.
Define c as a count of all the values in S smaller than i.
If $c = 0$, no such mapping exists. Otherwise, $j = c$
It should be noted that the post-processing must consider that the boundary conditions have been applied.

3.7. Aerodynamic Stiffness Matrix

For this section, only the component normal to the plate (the w displacement) will be considered. Thus:

$$\boldsymbol{N} = [N_1 \quad N_2 \quad \dots \quad N_8] \tag{46}$$

This project will only tackle panels at 0 angle of attack, so the equilibrium point of the panel will be 0. Additionally, the flow will be assumed to be along the x-axis of the panel. These assumptions will dramatically simplify the mathematics. Research should be done into Lyapunov if the reader is keen on exceeding these assumptions.
[8] gives Piston Theory as:

$$c_p(x,t) = \frac{2}{M_\infty^2}\left(\frac{v_n}{a_\infty} + \frac{\gamma+1}{4}\cdot\left(\frac{v_n}{a_\infty}\right)^2 + \frac{\gamma+1}{12}\cdot\left(\frac{v_n}{a_\infty}\right)^3\right) \tag{47}$$

$$\text{where } v_n = \dot{w} + V_\infty\left(\frac{\partial w}{\partial x} + \alpha_s\right)$$

To simplify, v_n will be reduced to:

$$v_n = V_\infty \frac{\partial w}{\partial x}$$

The linearisation of the equation and substituting for v_n leads to:

$$c_p(x,t) = \frac{2V_\infty}{M_\infty^2 a_\infty}\frac{\partial w}{\partial x} \tag{48}$$

The pressure coefficient is given as:

$$c_p = \frac{\Delta p}{\frac{1}{2}\rho V_\infty^2} = \frac{\Delta p}{q_\infty} \tag{49}$$

Equating (48) and (49):

$$\frac{\Delta p}{q_\infty} = \frac{2V_\infty}{M_\infty^2 a_\infty}\frac{\partial w}{\partial x}$$
$$\therefore \Delta p = \frac{2q_\infty V_\infty}{M_\infty^2 a_\infty}\frac{\partial w}{\partial x}$$

Since $M_\infty = \frac{v_\infty}{a_\infty}$

$$\Delta p = \frac{2q_\infty}{M_\infty}\frac{\partial w}{\partial x}$$

However, since these are at supersonic velocities, the Mach number is swapped for the Prandtl-Meyer compressibility corrected Mach number:

$$\Delta p = \frac{2q_\infty}{\beta}\frac{\partial w}{\partial x}$$
$$\text{where } \beta = \sqrt{M_\infty^2 - 1}$$

The parameter λ is defined as:

$$\lambda = \frac{2q_\infty}{\beta} \tag{50}$$

Thus:

$$\Delta p = \lambda\frac{\partial w}{\partial x}$$

From (19):

$$W = \int_{-1}^{1}\int_{-1}^{1} \lambda\frac{\partial w}{\partial x}\cdot w|\boldsymbol{J}|\, d\xi d\eta$$

Substituting:

$$w(x,y) = \boldsymbol{N}\boldsymbol{w}$$
$$\frac{\partial w(x,y)}{\partial x} = \frac{\partial \boldsymbol{N}}{\partial x}\boldsymbol{w} = \boldsymbol{w}^T\frac{\partial \boldsymbol{N}^T}{\partial x}$$
$$\therefore W = \lambda\int_{-1}^{1}\int_{-1}^{1} \boldsymbol{w}^T\frac{\partial \boldsymbol{N}^T}{\partial x}\,\boldsymbol{N}\boldsymbol{w}|\boldsymbol{J}|\, d\xi d\eta$$

Minimising with respect to the displacement using (21) and (23):

$$\frac{\partial W}{\boldsymbol{w}} = 0 = \lambda\int_{-1}^{1}\int_{-1}^{1}\frac{\partial \boldsymbol{N}^T}{\partial x}\,\boldsymbol{N}\boldsymbol{w}|\boldsymbol{J}|\, d\xi d\eta$$

Factoring $\boldsymbol{w}$ and λ to be in the form of (22), the aerodynamic stiffness matrix is then:

$$\boldsymbol{K}_a = \int_{-1}^{1}\int_{-1}^{1}\frac{\partial \boldsymbol{N}^T}{\partial x}\,\boldsymbol{N}|\boldsymbol{J}|\, d\xi d\eta \tag{51}$$

Since only the vertical displacements were considered, the other dofs will need to be included. Thus, the local aerodynamic stiffness matrix is padded with 0s. Care should be taken to ensure the vertical displacements are in the correct place. With MATLAB indexing, this would be every $3(n-1)+1$ dof for Reissner-Mindlin theory and $5(n-1)+3$ dof for FSDT.

3.8. Flutter Analysis Setup

Recall (22):

$$\boldsymbol{M}\ddot{\boldsymbol{d}} + (\boldsymbol{K} + \lambda\boldsymbol{K}_a)\boldsymbol{d} = 0$$

Assuming a displacement $\boldsymbol{D}$ which follows harmonic motion:

$$\boldsymbol{D} = \boldsymbol{A}\boldsymbol{e}^{pt}$$
$$\text{Where } p = \sigma + i\omega \tag{52}$$

p is the complex representation of the wave. **Appendix F** visualises the amplitude response in one spatial dimension. Flutter begins when $\sigma = 0$ and $\omega > 0$. Hence, when the real part of p is 0, flutter is said to be at a critical point. When $\sigma > 0$ and $\omega > 0$, the panel is post-flutter.

Taking the second time derivative of $\boldsymbol{D}$:

$$\ddot{\boldsymbol{D}} = \boldsymbol{A}p^2\boldsymbol{e}^{pt}$$

Substituting this assumption for **d**:

$$\boldsymbol{M}\ddot{\boldsymbol{D}} + (\boldsymbol{K} + \lambda\boldsymbol{K}_a)\boldsymbol{D} = 0$$
$$\therefore \boldsymbol{M}\boldsymbol{A}p^2\boldsymbol{e}^{pt} + (\boldsymbol{K} + \lambda\boldsymbol{K}_a)\boldsymbol{A}\boldsymbol{e}^{pt} = 0$$
$$(\boldsymbol{M}p^2 + (\boldsymbol{K} + \lambda\boldsymbol{K}_a))\boldsymbol{A}\boldsymbol{e}^{pt} = 0$$
$$det(\boldsymbol{M}p^2 + (\boldsymbol{K} + \lambda\boldsymbol{K}_a)) = 0$$

This is equivalent to:

$$eig\big((\boldsymbol{K} + \lambda\boldsymbol{K}_a), \boldsymbol{M}\big) \quad (53)$$

This yields p^2 and the mode shapes. If there is still some confusion on employing these, the setup is visualised in **Appendix G**.

3.9. Modal Reduction Technique

The Modal reduction technique approximates the modes and modeshapes of the flutter solution using the set of modes and modeshapes of the free vibration problem where $\lambda = 0$. This reduces repeatedly solving an nxn eigenvalue problem into repeatedly solving a lower dimensional problem. This allows the user to control the computational efficiency at a minimal cost of accuracy.

The following will be proved:

$$\boldsymbol{\phi}_i\boldsymbol{K}\boldsymbol{\phi}_j = 0 \;\forall\; i \neq j \quad (54)$$
$$\boldsymbol{\phi}_i\boldsymbol{M}\boldsymbol{\phi}_j = 0 \;\forall\; i \neq j \quad (55)$$

From (22), where $\lambda = 0$:

$$\boldsymbol{K}\boldsymbol{\phi}_i = p_i^2\boldsymbol{M}\boldsymbol{\phi}_i \quad (56)$$
$$\boldsymbol{K}\boldsymbol{\phi}_j = p_j^2\boldsymbol{M}\boldsymbol{\phi}_j \quad (57)$$

Multiplying (56) by $\boldsymbol{\phi}_j^T$ and (57) by $\boldsymbol{\phi}_i^T$:

$$\boldsymbol{\phi}_j^T\boldsymbol{K}\boldsymbol{\phi}_i = p_i^2\boldsymbol{\phi}_j^T\boldsymbol{M}\boldsymbol{\phi}_i \quad (58)$$
$$\boldsymbol{\phi}_i^T\boldsymbol{K}\boldsymbol{\phi}_j = p_j^2\boldsymbol{\phi}_i^T\boldsymbol{M}\boldsymbol{\phi}_j \quad (59)$$

Taking the transpose of (58):

$$\big(\boldsymbol{\phi}_i^T\boldsymbol{K}\boldsymbol{\phi}_j\big)^T = p_j^2\big(\boldsymbol{\phi}_i^T\boldsymbol{M}\boldsymbol{\phi}_j\big)^T \quad (60)$$
$$\boldsymbol{\phi}_j^T\boldsymbol{K}^T\boldsymbol{\phi}_i = p_j^2\boldsymbol{\phi}_j^T\boldsymbol{M}^T\boldsymbol{\phi}_i \quad (61)$$

Since **K** and **M** are symmetrical:

$$\boldsymbol{\phi}_j^T\boldsymbol{K}\boldsymbol{\phi}_i = p_j^2\boldsymbol{\phi}_j^T\boldsymbol{M}\boldsymbol{\phi}_i$$

Equating LHS of (61) and (59):

$$p_i^2\boldsymbol{\phi}_j^T\boldsymbol{M}\boldsymbol{\phi}_i = p_j^2\boldsymbol{\phi}_j^T\boldsymbol{M}\boldsymbol{\phi}_i$$
$$(p_i^2 - p_j^2)\boldsymbol{\phi}_j^T\boldsymbol{M}\boldsymbol{\phi}_i = 0$$

Therefore, $\boldsymbol{\phi}_j^T\boldsymbol{M}\boldsymbol{\phi}_i = 0 \;\forall\; i \neq j$. From (58), $\boldsymbol{\phi}_j^T\boldsymbol{K}\boldsymbol{\phi}_i = 0 \;\forall\; i \neq j$.

It will also be desired to normalise the modeshapes $\boldsymbol{\phi}$ into $\boldsymbol{\psi}$ such that:

$$\boldsymbol{\psi}_i^T\boldsymbol{M}\boldsymbol{\psi}_i = 1 \quad (62)$$

For (55), where $i = j$:

$$\boldsymbol{\phi}_i^T\boldsymbol{M}\boldsymbol{\phi}_i = \mu$$
$$\therefore \frac{\boldsymbol{\phi}_i^T\boldsymbol{M}\boldsymbol{\phi}_i}{\mu} = 1$$

This is equivalent to:

$$\frac{\boldsymbol{\phi}_i^T\boldsymbol{M}\boldsymbol{\phi}_i}{\sqrt{\mu}\times\sqrt{\mu}} = 1$$

Organising in this form:

$$\left(\frac{\boldsymbol{\phi}_i}{\sqrt{\mu}}\right)^T \boldsymbol{M}\left(\frac{\boldsymbol{\phi}_i}{\sqrt{\mu}}\right) = 1$$

Comparing this with (62), it is now simple to extract the new normalised modeshapes:

$$\boldsymbol{\psi}_i = \frac{\boldsymbol{\phi}_i}{\sqrt{\mu}} = \frac{\boldsymbol{\phi}_i}{\sqrt{\boldsymbol{\phi}_i^T \boldsymbol{M} \boldsymbol{\phi}_i}} \tag{63}$$

Now with all the preliminary knowledge, it is time to derive the modal reduction technique from [4]:

From (55) and (62): $\boldsymbol{\psi}^T \boldsymbol{M} \boldsymbol{\psi}$ is an identity matrix (at $i \neq j, \boldsymbol{\psi}_i^T \boldsymbol{M} \boldsymbol{\psi}_j = 0$ and $i = j, \boldsymbol{\psi}_i^T \boldsymbol{M} \boldsymbol{\psi}_j = 1$).

Thus:

$$\boldsymbol{\psi}^T \boldsymbol{M} \boldsymbol{\psi} = \boldsymbol{I} \tag{64}$$

Multiplying by $\boldsymbol{p}^2$:

$$\boldsymbol{\psi}^T \boldsymbol{p}^2 \boldsymbol{M} \boldsymbol{\psi} = \boldsymbol{p}^2 \mathbf{I}$$

Thus:

$$\boldsymbol{\psi}^T \boldsymbol{K} \boldsymbol{\psi} = \boldsymbol{p}^2 \mathbf{I} \tag{65}$$

Assume $\boldsymbol{\psi}$ contains the first m modeshapes associated with the largest eigenvalues of the free vibration problem with $\lambda = 0$.

The modeshapes $\boldsymbol{\psi}$ can then be used to approximate the solution of (22) when for any λ:

$$\boldsymbol{A} = \boldsymbol{\psi} \boldsymbol{\eta}$$

Premultiplying (22) by $\boldsymbol{\psi}^T$:

$$\left(\boldsymbol{\psi}^T \boldsymbol{K} \boldsymbol{\psi} + \lambda \boldsymbol{\psi}^{\mathrm{T}} \boldsymbol{K}_a \boldsymbol{\psi} - \boldsymbol{\psi}^T \boldsymbol{p}^2 \boldsymbol{M} \boldsymbol{\psi}\right) \boldsymbol{\eta} = \mathbf{0}$$

Rearranging:

$$\left(\boldsymbol{\psi}^T \boldsymbol{K} \boldsymbol{\psi} + \lambda \boldsymbol{\psi}^{\mathrm{T}} \boldsymbol{K}_a \boldsymbol{\psi}\right) \boldsymbol{\eta} = \left(\boldsymbol{\psi}^T \boldsymbol{p}^2 \boldsymbol{M} \boldsymbol{\psi}\right) \boldsymbol{\eta}$$

Using (64) and (65):

$$\left(\boldsymbol{p}^2 \mathbf{I} + \lambda \boldsymbol{\psi}^{\mathrm{T}} \boldsymbol{K}_a \boldsymbol{\psi}\right) \boldsymbol{\eta} = \left(\boldsymbol{p}^2 \mathbf{I}\right) \boldsymbol{\eta}$$

This can now be solved to give the aerodynamics included modes and modeshapes. Thus, (53) is replaced with:

$$eig(\boldsymbol{p}^2 \boldsymbol{I} + \lambda \boldsymbol{\psi}^T \boldsymbol{K}_a \boldsymbol{\psi}) \tag{66}$$

3.10. Flutter Results

This section will feature analysis of isotropic and laminate panels and comparison with first order piston theory. There will also be comparison with [10], which used third order piston theory. Unfortunately, due to limited space, the mode shapes will not be shown. Although note that these are highly valuable to designers in determining how to mitigate flutter. Convergence studies will also be included, where m stands for the number of modes.

Isotropic

[4] defines the following non-dimensional parameters for isotropic plates:

$$\lambda_{cr}^* = \frac{\lambda_{cr} A^3}{D} \tag{67}$$

$$\omega_{cr}^* = \frac{\omega_{cr}^2 \rho h A^4}{D} \tag{68}$$

Where $D = \frac{Eh^3}{12(1-\nu^2)}$

The first panel is an isotropic square panel with properties thickness to side length ratio: $\frac{h}{A} = 0.001$.This puts it in thin plate category. The results for SSSS are tabulated in Table 7. The results for CCCC are tabulated in Table 8.

Table 7: Results for isotropic SSSS compared with reference (3 s.f.)

m	λ_{cr}^*			ω_{cr}^*			
	15x15	**20x20**	**40x40**	**15x15**	**20x20**	**40x40**	←Mesh
5	500	500	500	1620	1610	1610	
10	507	505	505	1820	1820	1820	
15	516	505	506	1850	1820	1820	
20	516	514	514	1850	1850	1850	
25	513	512	512	1850	1840	1840	
30	514	512	512	1850	1845	1840	
35	514	513	513	1850	1850	1850	
40	514	513	513	1850	1850	1850	
50	514	513	512	1850	1850	1850	
Ref [4]		513			1850		
Ref [23]		513			1850		

Table 8: Results for isotropic CCCC compared with reference (3 s.f.)

m	λ_{cr}^*			ω_{cr}^*			
	15x15	**20x20**	**40x40**	**15x15**	**20x20**	**40x40**	←Mesh
5	731	717	717	3760	3700	3700	
10	857	841	841	4320	4250	4250	
15	872	841	841	4380	4250	4250	
20	871	856	856	4380	4310	4310	
25	869	853	853	4370	4300	4310	
30	870	853	853	4380	4300	4310	
35	870	854	854	4380	4300	4300	
40	870	854	854	4380	4300	4300	
50	870	854	854	4380	4300	4300	
Ref [4]		851			4290		
Ref [23]		850			4280		

Laminates

[4] tests square laminates, where h/A is the thickness to length ratio. [10] tests composites with varying ply angles. Table 9 details the material properties of these.

Table 9: Material properties for symmetric and asymmetric laminates [4]

Property	**Symmetric** [4]	**Asymmetric** [4]	**3rd Order** [10]
$E_L\ (GPa)$	100	213.7	54
$E_T\ (GPa)$	10	18.6	18
$G_{LT}, G_{TT}\ (GPa)$	3.3	5.17	7.2
ν_{LT}	0.3	0.28	0.3
h/A	0.001	0.05	0.0667
λ_{cr}^*	$\frac{\lambda_{cr}A^3}{D_{11}(0)}$	$\frac{\lambda_{cr}A^3}{E_T h^3}$	$\frac{\lambda_{cr}A^3}{D_{11}(0)}$
ω_{cr}^*	$\frac{\omega_{cr}^2 \rho h A^4}{D_{11}(0)}$	$\frac{\omega_{cr}^2 \rho h A^4}{E_T h^3}$	N/A
BC	SSSS	CCCC	SSSS

In Table 9, $D_{11}(0)$ is D_{11} from (37) when all the laminate angles are all 0. Table 10 displays the layups of the panels used by [4]. The results for the laminates are tabulated in Table 11. Figure 14 demonstrates the comparison between first order piston theory and third order piston theory employed by [10]. It plots the variation of λ_{cr}^* with θ, where the panel is defined by: $[\theta, -\theta, -\theta, \theta]$.

Table 10: Panel setups

Panel	**A**	**B**	**C**
Layup	0_6	$[+45/-45/+45]_s$	[+45/-45]

Table 11: Results for laminates compared with references (3 s.f.)

m	λ^*_{cr}			ω^*_{cr}			
	A	**B**	**C**	**A**	**B**	**C**	←Panel
5	285	176	136	884	702	590	
10	316	192	136	1170	751	632	
15	369	196	136	1145	753	632	
20	356	213	136	1116	765	645	
25	356	213	136	1128	812	692	
30	356	213	136	1128	813	692	
35	359	214	136	1128	813	692	
40	359	216	136	1128	813	692	
50	360	216	136	1128	813	692	
Ref [4]	359	216	139	1125	812	705	
Ref [24]	360	207					
Ref [25]			139			684	

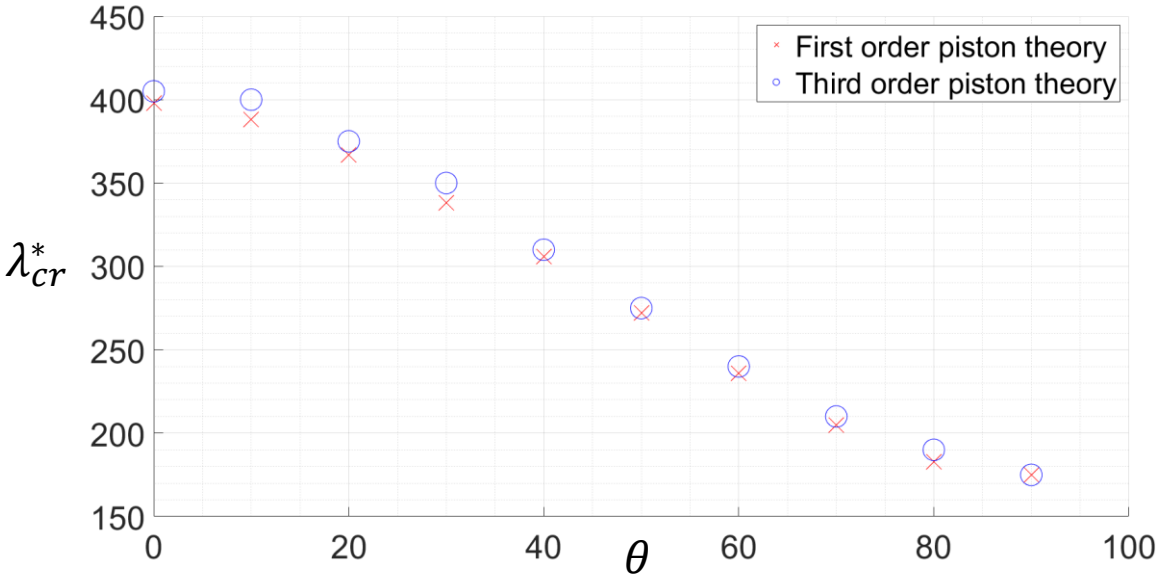

Figure 14: Comparisons between first order piston theory and third order piston theory by [10]

Discussion

Table 7 and Table 8 compare the Reissner-Mindlin approach against FSDT. There is good match between the data which gives good confidence in the implementation and assumptions made. Table 11 also gives good confidence in the FSDT implementation. Figure 14 compares first order piston theory against third order piston theory. Although they match quite well, first order piston theory underestimates λ^*_{cr} slightly. This is acceptable since it adds an additional safety factor to the predicted design. Overall, this demonstrates the power of first order piston theory as an initial design method. Finally, whilst no time study was done, each simulation took less than 5 seconds. This would not be easily possible using CFD.

4. Conclusion & Further work

To conclude, the project was an overall success, with results that match well with first order piston theory literature. It even compared well with [10] which used third order piston theory in NASTRAN. This gives confidence in the methods employed throughout this project. The solution times were also all less than 5 seconds, demonstrating the power of the sparse matrix approach, reduced integration scheme, frequency approach and modal reduction technique. This tool is not meant to replace commercial software as this is unrealistic. It is designed to aid researchers who want a simple tool to work with more fundamental theories.

The outputs of the code are the critical flutter Mach number, the modeshapes and frequencies. The critical flutter Mach number can be used to predict flutter occurrence whilst the modeshapes and frequencies can be used to formulate strategies to mitigate it.

Although not much innovation has been made in the topic, there is now a free usable tool to research supersonic/hypersonic panel flutter. Alternatively, this tool has a rigorous structural element so could be used for other structural research. Furthermore, the implementation is documented thoroughly in this paper. Admittedly, the code structure was sacrificed for time demands. Hence, to completely satisfy the aims, the code structure should be improved, and thorough documentation should be produced to guide users.

Further work involves including thermal effects, buckling, pre-stressed panels, other aerodynamic models and shells. Shells would be a major inclusion as it would allow the modelling of non-flat surfaces. However, it is believed that the detailed derivations in the paper should allow the reader to implement this in future if desired.

References

[1] Z. K and Z. M, "Flutter Analysis of A Laminated Composite Plate with Temperature Dependent Material Properties," *International Journal of Aeronautical Science & Aerospace Research*, pp. 106–114, Jun. 2016, doi: 10.19070/2470-4415-1600013.

[2] "NASA SPACE VEHICLE DESIGN CRITERIA A N D SPACE A D M I N i ST RAT i LI r\i," 1972.

[3] B. E. Eldon Kordes, W. J. Tuovila, and L. D. Guy SU, "Y NATIONAL AERONAUTICS AND SPACE ADMINISTRATION TECHNICAL NOTE D-451 FLUTTER RESEARCH ON SKIN PANELS."

[4] S. Wang, "High-supersonic/hypersonic flutter of prismatic composite plate/shell panels," *J Spacecr Rockets*, vol. 36, no. 5, pp. 750–757, 1999, doi: 10.2514/2.3489.

[5] "prior written consent of SpaceX," 2020.

[6] "Plate Geometry and Deformation."

[7] "Study and Comparison of Different Plate Theory," *International Journal of Engineering Research and Advanced Technology*, 2017, doi: 10.7324/ijerat.3130.

[8] J. J. Mcnamara and P. P. Friedmann, "Aeroelastic and Aerothermoelastic Analysis of Hypersonic Vehicles: Current Status and Future Trends," 2006.

[9] D. Q. Tsunematsu, M. V. Donadon, and V. L. Reis, "Explicit finite element method for nonlinear flutter analysis of composite panels," *Thin-Walled Structures*, vol. 165, Aug. 2021, doi: 10.1016/j.tws.2021.107964.

[10] V. Silva, D. Santos, H. De, A. Pegado, V. S. Dos Santos, and H. A. Pegado, "Use of Third-Order Piston Theory in Panel Flutter Analysis on Composite Laminated Plates with NASTRAN Electric Aircraft Structural Design View project Composite and Metal joints View project Use of Third-Order Piston Theory in Panel Flutter Analysis on Composite Laminated Plates with NASTRAN." [Online]. Available: https://www.researchgate.net/publication/346253587

[11] "Aeroelastic Analysis User's Guide Contents."

[12] Cheng, Guangfeng. 'Finite Element Modal Formulation for Panel Flutter at Hypersonic Speeds and Elevated Temperatures' (2002)", doi: 10.25777/0hkt-8x19.

[13] G. Cheng and C. Mei, "Finite Element Modal Formulation for Hypersonic Panel Flutter Analysis with Thermal Effects," *AIAA Journal*, vol. 42, no. 4, pp. 687–695, 2004, doi: 10.2514/1.9553.

[14] M. N. Bismarck-Nasr, "Finite element analysis of aeroelasticity of plates and shells."

[15] H. T. Thai and S. E. Kim, "A review of theories for the modeling and analysis of functionally graded plates and shells," *Composite Structures*, vol. 128. Elsevier Ltd, p. 70, Sep. 05, 2015. doi: 10.1016/j.compstruct.2015.03.010.

[16] H. T. Thai, T. K. Nguyen, T. P. Vo, and T. Ngo, "A new simple shear deformation plate theory," *Compos Struct*, vol. 171, pp. 277–285, Jul. 2017, doi: 10.1016/j.compstruct.2017.03.027.

[17] N. D. Phan and J. N. Reddy, "Analysis of laminated composite plates using a higher-order shear deformation theory," *Int J Numer Methods Eng*, vol. 21, no. 12, pp. 2201–2219, 1985, doi: 10.1002/nme.1620211207.

[18] Z. Priebe, A. H. Frank, K. Skolan, and F. Teknikvetenskap, "AN AEROELASTIC PREDICTION MODEL FOR SLENDER WINGS IN SUPERSONIC FLOW."

[19] A. Chama, S. Gerber, and R. J. Wang, "Newton-raphson solver for finite element methods featuring nonlinear hysteresis models," *IEEE Trans Magn*, vol. 54, no. 1, Jan. 2018, doi: 10.1109/TMAG.2017.2761319.

[20] J. Renze, Stover, Christopher, and E. W. Weisstein, "Inner Product," *Mathworld*, May 03, 2023.

[21] G. R. Liu and S. S. Quek, "Briefing on Mechanics for Solids and Structures," *The Finite Element Method*, pp. 13–41, 2014, doi: 10.1016/B978-0-08-098356-1.00002-3.

[22] S. Wang, "FREE VIBRATION ANALYSIS OF SKEW FIBRE-REINFORCED COMPOSITE LAMINATES BASED ON FIRST-ORDER SHEAR DEFORMATION PLATE THEORY," 1997.

[23] M. D. Olson, "Some flutter solutions using finite elements," *https://doi.org/10.2514/3.5751*, vol. 8, no. 4, pp. 747–752, May 2012, doi: 10.2514/3.5751.

[24] A. Barai, S. Durvasula, A. Barai, and S. Durvasula, "Flutter of Hybrid Laminated Flat Panels with Simply Supported Edges in Supersonic Flow," *JSV*, vol. 169, no. 3, pp. 373–386, Jan. 1994, doi: 10.1006/JSVI.1994.1023.

[25] C. L. Liao and Y. W. Sun, "Flutter analysis of stiffened laminated composite plates and shells in supersonic flow," *https://doi.org/10.2514/3.11865*, vol. 31, no. 10, pp. 1897–1905, May 2012, doi: 10.2514/3.11865.

Acknowledgements

Firstly, I would like to thank my supervisor for suggesting this topic and guiding me through it. Next, I would like to thank my family for supporting my passion since my youth. Finally, I would also like to thank my friends for providing a necessary balance to my life.

If I have seen further, it is by standing on the shoulders of giants – Isaac Newton

Appendix A

Quadratic shape function equation

$$\boldsymbol{\phi} = \begin{bmatrix} 1 & -1 & -1 & 1 & 1 & 1 & -1 & -1 \\ 1 & 1 & -1 & -1 & 1 & 1 & 1 & -1 \\ 1 & 1 & 1 & 1 & 1 & 1 & 1 & 1 \\ 1 & -1 & 1 & -1 & 1 & 1 & -1 & 1 \\ 1 & 0 & -1 & 0 & 0 & 1 & 0 & 0 \\ 1 & 1 & 0 & 0 & 1 & 0 & 0 & 0 \\ 1 & 0 & 1 & 0 & 0 & 1 & 0 & 0 \\ 1 & -1 & 0 & 0 & 1 & 0 & 0 & 0 \end{bmatrix} \begin{Bmatrix} \alpha_0 \\ \alpha_1 \\ \alpha_2 \\ \alpha_3 \\ \alpha_4 \\ \alpha_5 \\ \alpha_6 \\ \alpha_7 \end{Bmatrix}$$

Appendix B

Quadratic quadrilateral shape functions & code to generate shape functions

Shape Function Index	Shape Function Equation
N_1	$-(1-\eta)(1-\xi)(1+\xi+\eta)/4$
N_2	$-(1-\eta)(1+\xi)(1-\xi+\eta)/4$
N_3	$-(1+\eta)(1+\xi)(1-\xi-\eta)/4$
N_4	$-(1+\eta)(1-\xi)(1+\xi-\eta)/4$
N_5	$(1-\eta)(1-\xi)(1+\xi)/2$
N_6	$(1-\eta)(1+\xi)(1+\eta)/2$
N_7	$(1+\eta)(1-\xi)(1+\xi)/2$
N_8	$(1-\eta)(1-\xi)(1+\eta)/2$

```
syms xi eta
nodes = [-1, -1;
          1, -1;
          1, 1;
          -1, 1;
          0, -1;
          1, 0;
          0, 1;
          -1, 0];
uu = 0;
u = [];
N = sym('N', [8, 1])
A = zeros(8, 8);
u = sym('u', [8, 1]);
for i=1:8
    A(i, :) = [1, nodes(i, 1), nodes(i, 2), nodes(i, 1)*nodes(i, 2), nodes(i,
1)^2, nodes(i, 2)^2, nodes(i, 1) * nodes(i, 2)^2, nodes(i, 1)^2*nodes(i, 2)];
end
A
alpha = inv(A) * u;
eqn = [1 xi eta xi*eta xi^2 eta^2 xi*eta^2 xi^2*eta] * alpha
u1coeffs = eqn;
ucoeffs = repmat(eqn, [8, 1]);
for i=1:8
    for j=1:8
        if(i == j)
            ucoeffs(i) = subs(ucoeffs(i), u(j), 1);
        else
            ucoeffs(i) = subs(ucoeffs(i), u(j), 0);
        end
    end
end
```

Appendix C
Quadratic quadrilateral shape function derivatives

Shape Function Index	Shape Function Derivatives
$\frac{dN_1}{d\xi}$	$-0.25(\eta - 1)(\eta + \xi + 1) - 0.25(\eta - 1)(\xi - 1)$
$\frac{dN_1}{d\eta}$	$-0.25(\xi - 1)(\eta + \xi + 1) - 0.25(\eta - 1)(\xi - 1)$
$\frac{dN_2}{d\xi}$	$0.25(\eta - 1)(\eta - \xi + 1) - 0.25(\eta - 1)(\xi + 1)$
$\frac{dN_2}{d\eta}$	$0.25(\xi + 1)(\eta - \xi + 1) + 0.25(\eta - 1)(\xi + 1)$
$\frac{dN_3}{d\xi}$	$0.25(\eta + 1)(\eta + \xi - 1) + 0.25(\eta + 1)(\xi + 1)$
$\frac{dN_3}{d\eta}$	$0.25(\xi + 1)(\eta + \xi - 1) + 0.25(\eta + 1)(\xi + 1)$
$\frac{dN_4}{d\xi}$	$0.25(\eta + 1)(\xi - \eta + 1) + 0.25(\eta + 1)(\xi - 1)$
$\frac{dN_4}{d\eta}$	$0.25(\xi - 1)(\xi - \eta + 1) - 0.25(\eta + 1)(\xi - 1)$
$\frac{dN_5}{d\xi}$	$0.5(\eta - 1)(\xi - 1) + 0.5(\eta - 1)(\xi + 1)$
$\frac{dN_5}{d\eta}$	$0.5(\xi - 1)(\xi + 1)$
$\frac{dN_6}{d\xi}$	$-0.5(\eta - 1)(\eta + 1)$
$\frac{dN_6}{d\eta}$	$-0.5(\eta - 1)(\xi + 1) - 0.5(\eta + 1)(\xi + 1)$
$\frac{dN_7}{d\xi}$	$-0.5(\eta + 1)(\xi - 1) - 0.5(\eta + 1)(\xi + 1)$
$\frac{dN_7}{d\eta}$	$-0.5(\xi - 1)(\xi + 1)$
$\frac{dN_8}{d\xi}$	$0.5(\eta - 1)(\eta + 1)$
$\frac{dN_8}{d\eta}$	$0.5(\eta - 1)(\xi - 1) + 0.5(\eta + 1)(\xi - 1)$

Appendix D
Gauss Points for fully integrated quadratic quadrilateral elements

The basis is:

$$[1, x, x^2, x^3]$$

From the reduced scheme, the first 3 L_m are:

$$[1, x, x^2 - \frac{1}{3}]$$

$$x^3 - 1 \cdot \frac{\int_{-1}^{1} 1 \cdot x^3 \, dx}{\int_{-1}^{1} 1 \cdot 1 \, dx} - x \cdot \frac{\int_{-1}^{1} x \cdot x^3 \, dx}{\int_{-1}^{1} x \cdot x \, dx} - (x^2 - \frac{1}{3}) \cdot \frac{\int_{-1}^{1} (x^2 - \frac{1}{3}) \cdot x^3 \, dx}{\int_{-1}^{1} (x^2 - \frac{1}{3}) \cdot (x^2 - \frac{1}{3}) \, dx} = x^3 - \frac{3x}{5}$$

The Gauss points are then the roots of: $x^3 - \frac{3x}{5} = 0$. Or: $\pm\sqrt{\frac{3}{5}}$ and 0.

Doing a similar process as the reduced scheme, but with a quadratic polynomial:

$$\begin{bmatrix} 1 & 1 & 1 \\ x_1 & x_2 & x_3 \\ x_1^2 & x_2^2 & x_3^2 \end{bmatrix} \begin{bmatrix} w_1 \\ w_2 \\ w_3 \end{bmatrix} = \begin{bmatrix} 2 \\ 0 \\ 2 \\ \frac{2}{3} \end{bmatrix}$$

Substituting the corresponding Gauss Points for x_1, x_2 and x_3:

$$\begin{bmatrix} 1 & 1 & 1 \\ -\sqrt{\frac{3}{5}} & 0 & \sqrt{\frac{3}{5}} \\ \left(-\sqrt{\frac{3}{5}}\right)^2 & 0 & \left(\sqrt{\frac{3}{5}}\right)^2 \end{bmatrix} \begin{bmatrix} w_1 \\ w_2 \\ w_3 \end{bmatrix} = \begin{bmatrix} 2 \\ 0 \\ 2 \\ \frac{2}{3} \end{bmatrix}$$

With $x_1 = -\sqrt{\frac{3}{5}}$, $x_2 = 0$ and $x_3 = \sqrt{\frac{3}{5}}$, the weights are:

$$w_1 = 5/9, w_2 = 8/9 \text{ and } w_3 = 5/9$$

Appendix E

Gauss Points and their corresponding weights

	Reduced		**Full**		
Weights	1	1	5/9	8/9	5/9
Position	$-\sqrt{\frac{1}{3}}$	$\sqrt{\frac{1}{3}}$	$-\sqrt{\frac{3}{5}}$	0	$\sqrt{\frac{3}{5}}$

Appendix F

Amplitude response shapes with varying ω and σ & code

	$\omega = 0$	$\omega > 0$
$\sigma < 0$	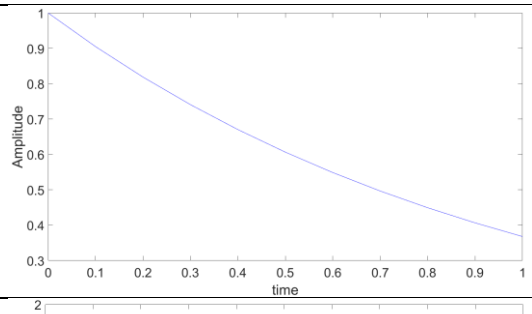	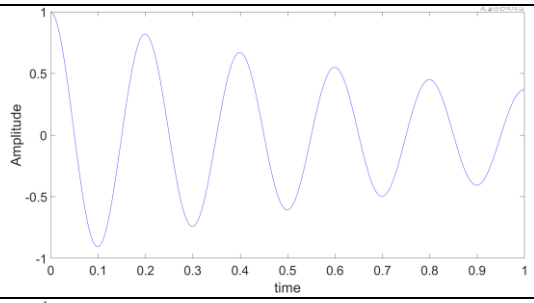
$\sigma = 0$	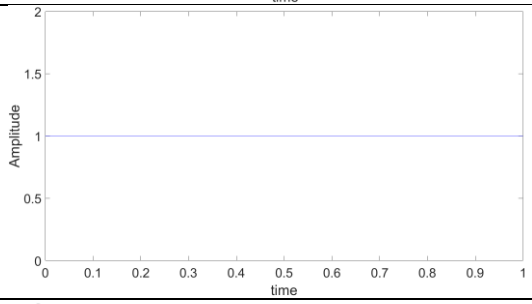	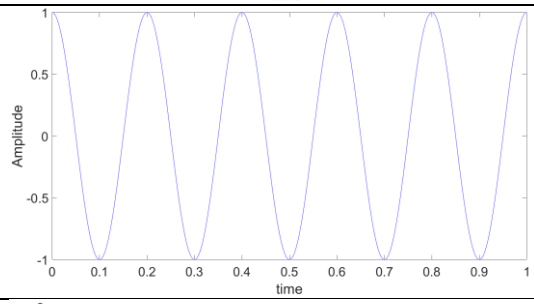
$\sigma > 0$	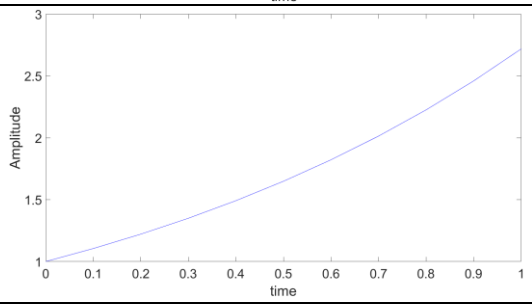	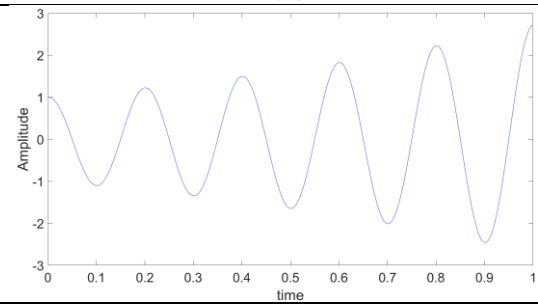

Appendix G
Setup visual aid

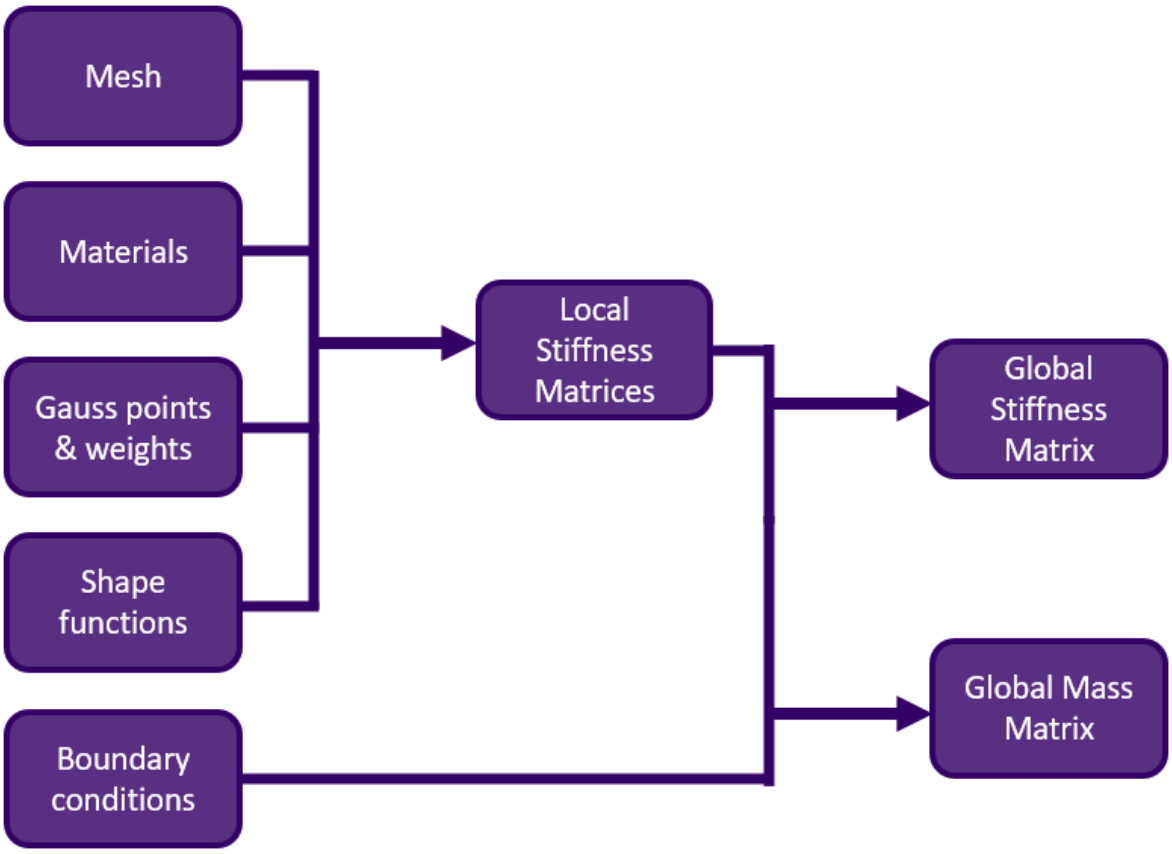

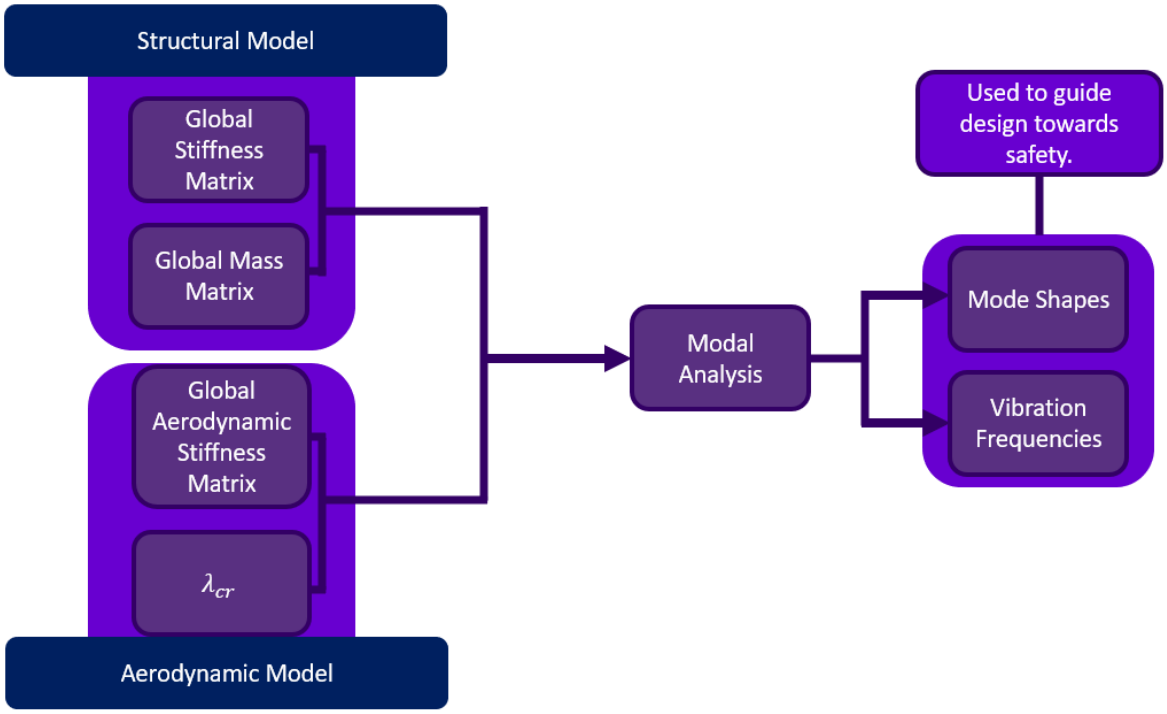

Algorithm 1 Flutter Solution

```
procedure SUPERSONIC FLUTTER SOLUTION
    Input: lambdas,shapefunctions, mesh, numberofmodes
    Output: λ_cr, ω_cr
    K = generateglobalstiffnessmatrix(shapefunctions, mesh)
    M = generateglobalmassmatrix(shapefunctions, mesh)
    K_a = generateglobalaerodynamicstiffnessmatrix(shapefunctions, mesh)
    [psi, eigenvalues] = freevibrationproblem(K, M, numberofmodes)
    psinormalised = normalisemodeshapes(psi)
    reducedmatrix = transpose(psinormalised) * K_a * psinormalised
    for lambda in lambdas do
        psquared = eig(eigenvalues + lambda * reducedmatrix)
        p = √psquared
        ω_cr = Imag(p)
        if Real(p) > 0 or Real(p) is 0 then
            return λ_cr, ω_cr
    return −1
```

Meeting Logs Semester 1

Weeks 1&2 were before first meeting.

19th October

Investigating Hypersonic/supersonic flutter of panels. Read Prof. Simon Wang's paper.

27th October

Look at capabilities of FEM software such as NASTRAN / ANSYS.

2nd November

Continue research. Went through ethics form.

9th November

Continue research.

16th November

Submitted title: "Investigating hypersonic flutter on panels in Finite Element Analysis"

Continue reading and writing report. Likely to use MATLAB for analysis.

23rd November

Discussed theories, such as element types etc. Organise ideas and write.

Talal Bukhamas

Simon Wang 28/11/2022

Meeting Summary Semester 2

Meetings were held every week except on the 8th of February and during the Easter holiday. Overall, the project was going well, so the main takeaway from each meeting was to continue work and to carry on research. There was a bit of issues risen from FSDT, however, this was a simple bug in the code and fixed and verified within a few weeks.

Ethics Awareness Form for Taught Student Projects

Project Title/Topic:

Investigation of Hypersonic Panel Flutter with the Finite Element Method using Plate Elements

---

All students should discuss with their supervisor whether their project might conflict with the University's ethical principles which can be found in the Ethical Policy Framework.

Students should complete the second column in the table below, discussing with their supervisor as appropriate.

Aspect of project	Does the project involve this aspect? (Yes / No)	If Yes, follow the process(es) below
Investigations with human participants and activity falling under the Human Tissue Act	No	1. Complete the Ethical Quick Test 2. Follow the process outlined on the HPSC Website
Military Applications, Dual Use Technologies or Security Sensitive Research	No	1. Complete the Ethical Quick Test 2. Follow the process outlined in Appendix 4
Accessing potentially security-sensitive material (e.g. online terrorist content or materials)	No	1. Complete the Ethical Quick Test 2. Follow the process outlined in Appendix 5
Funding by philanthropic gifts	No	Follow the process outlined in Appendix 6
Animal testing	No	Contact the Research Governance Officer: researchpolicy@lboro.ac.uk
Possible conflict with ethical principles partially or wholly outside the above.	No	1. Complete the Ethical Quick Test

Student Declaration

I confirm that I have discussed the ethics awareness form with my supervisor and, if appropriate, followed the relevant guidance / made the relevant application.

Student name: Talal Bukhammas

Student ID number: B930160

Signature: Talal Bukhammas

Date: 02/10/2022

Supervisor Declaration

I confirm that I have discussed the ethics awareness form with my supervisee and, if appropriate, requested that they follow the relevant guidance / make the relevant application.

Supervisor name:

Signature: Simon Wang

Date: 28/11/2022